Eidgenössische Technische Hochschule Zürich
Swiss Federal Institute of Technology Zurich

Seminar for Applied Mathematics SAM

Electromagnetic Port Boundary Conditions: Topological and Variational Perspective

R. Hiptmair and J. Ostrowski

Research Report No. 2020-27

May 2020
Latest revision: December 2020

Seminar für Angewandte Mathematik
Eidgenössische Technische Hochschule
CH-8092 Zürich
Switzerland

Submitted to Int. J. Numerical Modelling

Electromagnetic Port Boundary Conditions: Topological and Variational Perspective

R. Hiptmair[1] | J. Ostrowski[2]

[1]SAM, ETH Zurich, Rämistrasse 101, CH-8092 Zurich
[2]ABB Switzerland Ltd., Corporate Research, Segelhofstrasse 1, CH-5405 Baden

Correspondence
Ralf Hiptmair, Email:
hiptmair@sam.math.ethz.ch

Abstract

We present a comprehensive and variational approach to the coupling of electromagnetic field models with circuit-type models. That coupling relies on integral non-local quantities like voltage and current for electric ports, magnetomotive force and magnetic flux for magnetic ports, and linked currents and fluxes for "tunnels" in the field domain. These quantities are closely linked to non-bounding cycles studied in algebraic topology and they respect electromagnetic power balance laws. We obtain two dual variational formulations, called $\mathbf{E}$-based and $\mathbf{H}$-based, which provide a foundation for finite-element Galerkin discretization.

KEYWORDS:
field-circuit coupling, (M)ECE models, relative co-homology, electric and magnetic ports, finite elements

1 | INTRODUCTION

A central issue in computional electromagnetics is the coupling of full field descriptions of electromagnetic phenomena used in one region of space ("field domain") with "lumped-element" circuit models (network models/graphical models) in another region of space ("circuit domain"). Both talk to each other through well-defined zones on the interface, known as ports, terminals, or contacts. Details are given in Section 2.

In this article we present a *comprehensive* and *variational treatment* of this coupling based on the two ideas that have emerged as the underpinning of modern field-circuit coupling approaches:

(I) Electric and/or magnetic coupling between field and circuity domain is entirely channeled through the ports. We discuss the profound consequences in Section 3.1.

(II) The coupling through ports can completely be described by integral/non-local field quantities, see Section 5 for explanations.

In particular, this approach paves the way for introducing any kind of "lumped parameter excitations" into full Maxwell field models both in time and frequency domain. It permits us to imposed voltages, currents, and linked fluxes in the most general fashion.

Of course, also this work stands on the shoulders of giants, in particular on those of Alain Bossavit, whose 2000 seminal article on "Most general non-local boundary conditions for the Maxwell equations in a bounded region" [1] developed several key ideas that also pervade this work. The most important is the insight that non-local coupling quantities are of *topological nature* and closely connected to profound mathematical concepts investigated in (co-)homology theory a field of algebraic topology. We will explain this in Section 3.2. It is a pity that, probably owing to "inscrutable mathematics", A. Bossavit's topology-centered perspective has not received due attention. An exception is the work by L. Kettunen and S. Suuriniemi [2, 3]. What their work has in common with ours is the appreciation of the role of the fine structure of homology spaces, see Section 3.2.

Another fundamental idea from [1] is the connection between topological (Poincaré) duality and integration by parts, which we will discuss in Section 4. As a consequence, energy/power balance laws naturally emerge, commensurate with their central role in field-circuit coupling, highlighted, for instance, in [4] and [5].

We acknowledge that the above coupling "axioms" (II) and (I) have also been proposed by G. Ciuprina, D. Ioan and co-workes to lay the foundations of the so-called (M)ECE-technique for defining and classifying port conditions, see [6, 7, 8] and [9, Sect. 5.2.1]. These works, extending the final paragraph of [1], also link non-local boundary conditions with discretizations of Maxwell's equations. We will address this in Section 6. Of course, scores of other articles in computational electromagnetics have been devoted to the treatment of field-cicuit coupling. Most of them are mainly interested in special cases ("voltage excitation/current excitation") and are confined to quasi-static settings, see [4, 5, 10, 11, 12, 13, 14, 15] to name only a few contributions.

Our main contribution consists in the synthesis of all these ideas and their elaboration in a *function-space variational framework*, leading to the all-encompassing variational equations (36, "$\mathbf{E}$-based") and (39, "$\mathbf{H}$-based"), which involve only the physical fields and avoid introducing any potentials. They cover *all* possible port-associated excitations including a "topological" inductive coupling through linked fluxes. The variational formulations can serve as a natural starting point for Galerkin discretization and, subsequently, computer implementation. Thus, this work provides software developers in computational electromagnetics with an *algorithm*, that is, a clearly defined sequence of steps, for the treatment of field-circuit coupling in full generality.

We deliberately opted for a rather mathematical treatment and hope that we have kept the right balance of intuitive and rigorous arguments. In any case, in the final Section 7 we discuss a very concrete circuit-field coupling problem in frequency domain, in order to demonstrate how to extract a relevant $\mathbf{E}$-based finite-element model employing our general ideas.

2 | GEOMETRIC SETTING

We consider the linear Maxwell's equations governing the evolution of electromagnetic fields on a *bounded Lipschitz domain* $\Omega \subset \mathbb{R}^3$, which we call the "field domain". As in the introduction of [1], it is coupled to the rest of the universe through its boundary $\Gamma := \partial\Omega$, which is *partitioned* into four different parts:

$$\overline{\Gamma} = \overline{\Gamma}_E \cup \overline{\Gamma}_M \cup \overline{\Gamma}_I \cup \overline{\Gamma}_R \,,$$

with mutually disjoint interior and piecewise smooth boundaries. Here Γ_E designates the area occupied by **E**lectric contacts, Γ_M stands for **M**agnetic contacts, Γ_I is an **I**nsulated part of the boundary, and Γ_R is an artificial boundary on which **R**adiation conditions are to be imposed.

The contact boundaries have to be topologically simple in the sense of the following assumption.

Assumption 1. (i) Both Γ_E and Γ_M are the union of *topologically trivial* ports

$$\Gamma_E = \Gamma_E^1 \cup \cdots \cup \Gamma_E^{N_E} \quad , \quad \Gamma_M = \Gamma_M^1 \cup \cdots \cup \Gamma_M^{N_M} \,, \quad N_E, N_M \in \mathbb{N}_0 \,,$$

all of which have a positive distance from each other.

(ii) The radiation boundary is strictly separated from the other parts of Γ.

Here, topogically trivial means that the ports are simply connected (homeomorphic to a disk). The reader can imagine them as images of disks under bi-Lipschitz mappings.

A typical situation is sketched in Figure 1a. Complicated electric circuits occupy a region of space, the "circuit domain" Ω_C, which is tiny compared to the characteristic electromagnetic wavelength. They interact with the electromagnetic fields outside, where wave propagation cannot be neglected. The unbounded domain $\mathbb{R}^3 \setminus \overline{\Omega}_C$ is truncated to Ω and the impact of truncation is taken into account by absorbing boundary conditions on Γ_R.

Of course, the situation could be reversed with Ω a bounded cavity in Ω_C, see Figure 1b and [8, Sect. 2]. This can be appropriate when using the full Maxwell's equations locally in order to take into account both capacitive and inductive effects, though wave propagation may not be important. In Section 7 we will document a numerical simulation in such a setting.

For the bulk of our considerations the truncation by Γ_R does not matter much, and, thus, in large parts of the remainder of this article we just ignore the radiation boundary: We assume $\Gamma_R = \emptyset$. In addition, for the sake of simplicity we deal with connected circuit domains only, which implies that $\Gamma = \overline{\Gamma}_E \cup \overline{\Gamma}_M \cup \overline{\Gamma}_I = \partial\Omega_C$ is connected, too.

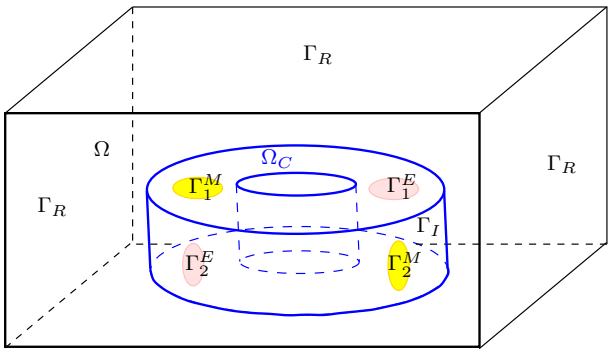

(a) Bounded circuit domain Ω_C: radiation conditions are imposed on the surface Γ_R of the artificial computational domain Ω (black box), the other boundary parts couple to Ω_C (blue hollow cylinder)

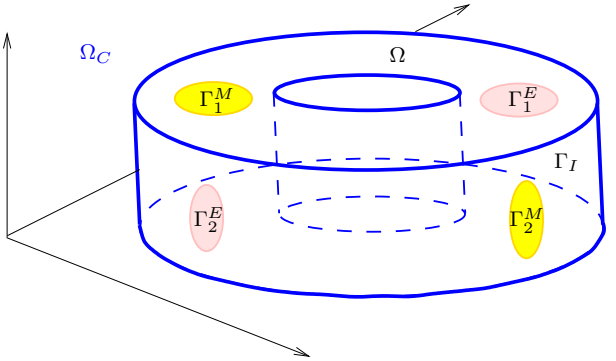

(b) Exterior circuit domain Ω_C, which is the unbounded complement of the bounded field domain Ω, here represented by the blue hollow cylinder.

FIGURE 1 Two typical situations compliant with Assumption 1 ($N_E = N_M = 2$)

3 | BOUNDARY CONDITIONS

3.1 | Function Spaces for Electromagnetic Fields

Recall that the space of finite-energy electric and magnetic fields in Ω is the Sobolev space[1]

$$\boldsymbol{H}(\mathbf{curl},\Omega) := \{\mathbf{v} \in \boldsymbol{L}^2(\Omega) : \ \mathbf{curl}\,\mathbf{v} \in \boldsymbol{L}^2(\Omega)\} \ .$$

To take into account the ports in a variational setting, we rely on two special closed subspaces. Their definition involves the two tangential traces

$$\boldsymbol{\gamma_t}\mathbf{u}(\boldsymbol{x}) := \boldsymbol{n}(\boldsymbol{x}) \times (\mathbf{u}(\boldsymbol{x}) \times \boldsymbol{n}(\boldsymbol{x})) \quad , \quad \gamma_\times \mathbf{u}(\boldsymbol{x}) := \mathbf{u}(\boldsymbol{x}) \times \boldsymbol{n}(\boldsymbol{x}) \ , \quad \boldsymbol{x} \in \Gamma \ ,$$

first defined for smooth vectorfields and then extended to continuous surjective mappings $\boldsymbol{\gamma_t} : \boldsymbol{H}(\mathbf{curl},\Omega) \to \boldsymbol{H}^{-\frac{1}{2}}(\mathrm{curl}_\Gamma,\Gamma)$ and $\boldsymbol{\gamma}_\times : \boldsymbol{H}(\mathbf{curl},\Omega) \to \boldsymbol{H}^{-\frac{1}{2}}(\mathrm{div}_\Gamma,\Gamma)$, respectively [17, Thm. 1]. Note that products of these two traces yield "Poynting vectors", that is power-flux two-forms: $\boldsymbol{\gamma_t}\mathbf{E} \cdot \boldsymbol{\gamma}_\times \mathbf{H} = (\mathbf{E} \times \mathbf{H}) \cdot \boldsymbol{n}|_\Gamma$. This is closely related to the integration by parts formula

$$\int_\Omega \mathbf{U} \cdot \mathbf{curl}\,\mathbf{V} - \mathbf{curl}\,\mathbf{U} \cdot \mathbf{V}\,\mathrm{d}\boldsymbol{x} = \int_{\partial\Omega} \boldsymbol{\gamma}_\times \mathbf{U} \cdot \boldsymbol{\gamma_t}\mathbf{V}\,\mathrm{d}S \quad \forall \mathbf{U},\mathbf{V} \in \boldsymbol{H}(\mathbf{curl},\Omega) \ , \tag{1}$$

and the fact that the trace spaces $\boldsymbol{H}^{-\frac{1}{2}}(\mathrm{curl}_\Gamma,\Gamma)$ and $\boldsymbol{H}^{-\frac{1}{2}}(\mathrm{div}_\Gamma,\Gamma)$ are in duality with respect to the $\boldsymbol{L}^2(\Gamma)$-inner product [17, Thm. 2].

Now we can introduce the key function spaces

- for electric fields (space "E" in [1], see also [8, Sect. 2])

$$\mathcal{V}_E := \{\mathbf{E} \in \boldsymbol{H}(\mathbf{curl},\Omega) : \ \boldsymbol{\gamma_t}\mathbf{E} = 0 \text{ on } \Gamma_E \ , \ \mathrm{curl}_\Gamma\, \boldsymbol{\gamma_t}\mathbf{E} = 0 \text{ on } \Gamma_I\} \ , \tag{2}$$

- and for the magnetic field (space "H" in [1])

$$\mathcal{V}_M := \{\mathbf{H} \in \boldsymbol{H}(\mathbf{curl},\Omega) : \ \boldsymbol{\gamma}_\times \mathbf{H} = 0 \text{ on } \Gamma_M \ , \ \mathrm{div}_\Gamma \boldsymbol{\gamma}_\times \mathbf{H} = 0 \text{ on } \Gamma_I\} \ , \tag{3}$$

Recall that the scalar-valued surface differential operators curl_Γ and div_Γ for tangential traces are defined as

$$\mathrm{curl}_\Gamma(\boldsymbol{\gamma_t}\mathbf{V}) = \mathrm{div}_\Gamma(\boldsymbol{\gamma}_\times \mathbf{V}) = \gamma_{\boldsymbol{n}}(\mathbf{curl}\,\mathbf{V}) \quad \text{for} \quad \mathbf{V} \in \boldsymbol{H}(\mathbf{curl},\Omega) \ , \tag{4}$$

$\gamma_{\boldsymbol{n}}$ the normal components trace, which immediately gives them a meaning for tangential vectorfields in the trace spaces $\boldsymbol{H}^{-\frac{1}{2}}(\mathrm{curl}_\Gamma,\Gamma)$ and $\boldsymbol{H}^{-\frac{1}{2}}(\mathrm{div}_\Gamma,\Gamma)$, respectively, as hinted by the notations.

What motivates the choice of the spaces $\mathcal{V}_E$ and $\mathcal{V}_M$? As for an electric contact $\Gamma_E^k \subset \Gamma_E$ you may think of a perfect conductor being attached to Ω, from which any electric field is expelled: $\boldsymbol{\gamma_t}\mathbf{E}|_{\Gamma_E} = 0$ for the electric field $\mathbf{E} \in \boldsymbol{H}(\mathbf{curl},\Omega)$. Similarly, the magnetic field $\mathbf{H}$ is suppressed at

[1] Concerning function spaces we adhere to notational conventions widely adopted in the mathematical analysis of numerical methods in computational electromagnetism, see [16, Ch. 3] and also [17, Sect. 2] for more exotic trace spaces. The space $\boldsymbol{H}(\mathbf{curl},\Omega)$ can be viewed as the "space of piecewise differentiable, tangentially continuous vectorfields".

the magnetic contact zones Γ_M^ℓ: $\boldsymbol{\gamma}_\times \mathbf{H}|_{\Gamma_M} = 0$. Conversely, the insulating interface Γ_I cannot be penetrated by any fluxes , neither magnetic nor electric, which, in light of (4), is enforced by the boundary conditions built into the definitions (2) and (3) of $\mathcal{V}_E$ and $\mathcal{V}_M$.

Remark 1. At the radiation boundary we assume general linear impedance boundary conditions

$$\boldsymbol{\gamma}_t \mathbf{E} = \mathsf{Z}(\boldsymbol{\gamma}_\times \mathbf{H}) \quad \text{on} \quad \Gamma_R \,, \tag{5}$$

where Z is a suitable invertible linear operator, possibly *non-local both in space and time*, meant to offset the effect of truncation approximately. Therefore, (5) is often called an absorbing boundary condition. Note that the boundary conditions at Γ_R do not show up neither in the space $\mathcal{V}_E$ nor in $\mathcal{V}_M$.

3.2 | Tool: (Co-)Homology

Co-homology and its dual theory, homology, is key to understanding obstructions to the existence of potential representations for functions in the kernel of differential operators, that is, obstructions to being in the range of other differential operators. This issue arises here, because both (2) and (3) define $\mathcal{V}_E$ and $\mathcal{V}_M$ as kernels of the surface differential operators curl_Γ and div_Γ, respectively.

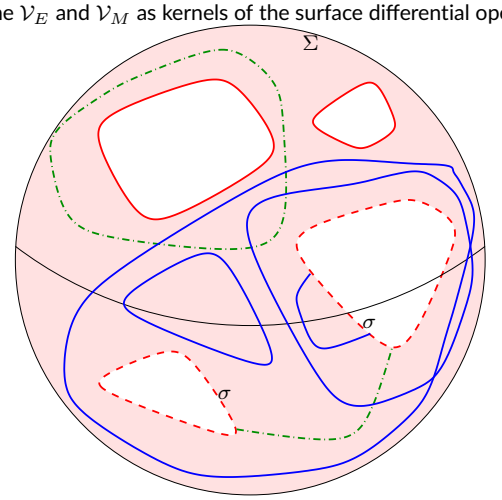

FIGURE 2 Γ is the surface of a sphere, Σ the pink area, the dashed - - - sections of its boundary constitute σ. The blue and green curves are σ-relative *cycles* in Σ. The blue cycles are *bounding*, the green are *not bounding*, both relative to σ.

(Co-)homology centers around the concepts of "cycle" and "boundary". We give an intuitive and geometric description, which, nevertheless captures their essence. A slightly more formal treatment from the perspective of chain calculus is offered in the introduction of [1].

Consider a non-degenerate[2] subset $\Sigma \subset \Gamma$ with sufficiently regular boundary. In addition, let σ denote a non-degenerate part of the boundary $\partial\Sigma$.

Definition 1 (Cycle). A σ-relative *cycle* $\gamma \subset \Sigma$ is a directed curve, which is either a loop (closed curve) or is open and has both its endpoints located on σ.

Definition 2 (Bounding). A σ-relative cycle γ is *bounding*, if there is a non-degenerate area $S \subset \Sigma$ such that $\gamma = \partial S \setminus \sigma$.

Examples of bounding and non-bounding cycles are visualized in Figure 2 taking the cue from [1, Fig. 1].

The following is a rephrasing of a fundamental result of (relative) co-homology theory for 2-surfaces concerning potential representations for the space of tangential vectorfields

$$\mathcal{W} := \left\{ \mathbf{v} \in \boldsymbol{H}(\mathrm{curl}_\Gamma, \Sigma) : \begin{array}{l} \mathrm{curl}_\Gamma \, \mathbf{v} = 0 \text{ in } \Sigma \,, \\ \mathbf{v} \text{ has vanishing tangential components on } \sigma \end{array} \right\} \tag{6}$$

based on the space of scalar functions

$$\mathcal{S} := \{ \varphi \in H^1(\Sigma) : \ \varphi|_\sigma = 0 \} \,. \tag{7}$$

Theorem 1. There is a number $N \in \mathbb{N}_0$ and a finite set of

(i) non-bounding (relative to σ) *fundamental σ-relative cycles* $\gamma_1, \ldots, \gamma_N$,

(ii) tangential co-homology vectorfields $\mathbf{c}_1, \ldots, \mathbf{c}_N \in \mathcal{W}$ satisfying

$$\int_{\gamma_j} \mathbf{c}_m \cdot \mathrm{d}s = \begin{cases} 1 & \text{for } m = j \,, \\ 0 & \text{else,} \end{cases} \qquad j, m \in \{1, \ldots, N\} \,, \tag{8}$$

[2] Non-degenerate means that the closure of the interior of Σ in Γ must coincide with $\overline{\Sigma}$.

such that, with $\mathcal{W}$ and $\mathcal{S}$ as in (6) and (7),

$$\mathcal{W} := \mathbf{grad}_\Gamma \mathcal{S} + \mathrm{span}\{\mathbf{c}_1, \ldots, \mathbf{c}_N\} \,. \tag{9}$$

Remark 2. The "$\frac{\pi}{2}$-rotated setting": If curl_Γ in (6) is replaced with div_Γ, then $\mathbf{curl}_\Gamma$ should substitute $\mathbf{grad}_\Gamma$ in (9).

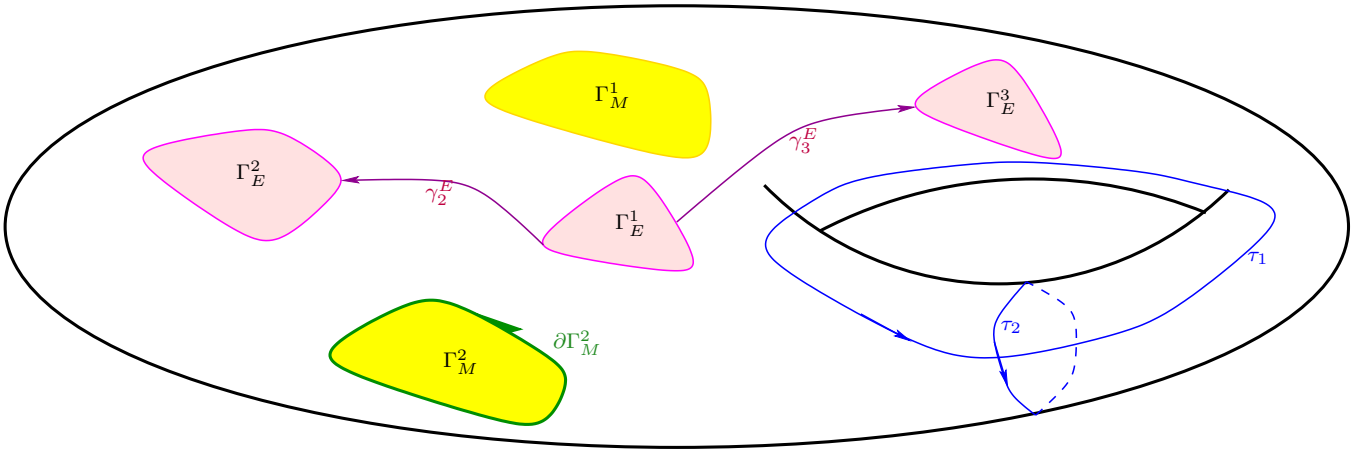

FIGURE 3 Torus-shaped Ω_C ($N_T = 2$); $N_E = 3$ electric ports in pink, $N_M = 2$ magnetic ports in yellow, fundamental cycles for the **relative homology space** $H_1(\Gamma_I, \partial\Gamma_E)$ are the "topological cycles" τ_1, τ_2 of class (T) in blue, the "electric connector cycles" γ_2^E, γ_3^E of class (CE) in purple, and the "magnetic port cycles" $\partial\Gamma_M^2$ of class (PE) in green.

Remark 3. We point out that Theorem 1 remains valid when replacing $\boldsymbol{H}(\mathrm{curl}_\Gamma, \Sigma)$ with $\boldsymbol{H}^{-\frac{1}{2}}(\mathrm{curl}_\Gamma, \Sigma)$ in (6) and $H^1(\Sigma)$ with $H^{\frac{1}{2}}(\Sigma)$ in (7), though zero boundary conditions on σ have to be rephrased as the existence of a zero extension in this case.

Remark 4. In homology theory the cycles $\gamma_1, \ldots, \gamma_N$ mentioned in Theorem 1 are introduced as 1-chains that form a basis of the relative homology space $H_1(\Sigma, \sigma)$. From this perspective, the vector fields $\mathbf{c}_1, \ldots, \mathbf{c}_N$ should be regarded as 2D Euclidean 1-form vector proxies of representatives of a basis of the relative co-homology space $H^1(\Sigma, \sigma)$, [18, Sect. 2 & 5].

Let us return to the geometric setting outlined in the introduction and to the space $\mathcal{V}_E$ from (2). Using the notation established above, as regards the application of Theorem 1 to $\mathcal{V}_E$ we face the situation $\Sigma = \Gamma_I$ and $\sigma = \partial\Gamma_E$. We need a precise characterization of the σ-relative cycles γ_i. As has already been realized in [3, Sect. III.C], the fundamental cycles **non-bounding relative to $\boldsymbol{\partial\Gamma_E}$** fall into three different classes, see Figure 3 (also for the color code):

(T) Fundamental non-bounding cycles ("topological cycles")

$$\tau_1, \ldots, \tau_{N_T} \,, \quad N_T := 2\beta_1(\Omega_C) \,,$$

of Γ, where $\beta_1(\Omega_C)$ is the first Betti number of Ω_C, that is, the number of handles/tunnels of both the circuit domain Ω_C and the field domain Ω.

(CE) $N_E - 1$ directed curves $\gamma_2^E, \ldots, \gamma_{N_E}^E \subset \Gamma_I$ connecting Γ_E^1 with the other electric ports $\Gamma_E^2, \ldots, \Gamma_E^{N_E}$ ("electric connector cycles"),

(PE) the $N_M - 1$ oriented boundaries $\partial\Gamma_M^\ell$, $\ell = 2, \ldots, N_M$, of the magnetic ports $\Gamma_M^2, \ldots, \Gamma_M^{N_M}$ ("magnetic port cycles").

Hence, the number of Γ_E-relative fundamental cycles is

$$N := N_T + \max\{N_M, 1\} + \max\{N_E, 1\} - 2 \,, \tag{10}$$

and, by Theorem 1, it takes that many co-homology tangential vectorfields to fill the gap between $\mathcal{V}_E$ and gradients of functions that vanish on $\partial\Gamma_E$.

The considerations for $\mathcal{V}_M$ invoke **$\boldsymbol{\Gamma_M}$-relative** homology. Again, three different classes of Γ_M-relative fundamental cycles can be identified in addition to class (T) from above, see Figure 4:

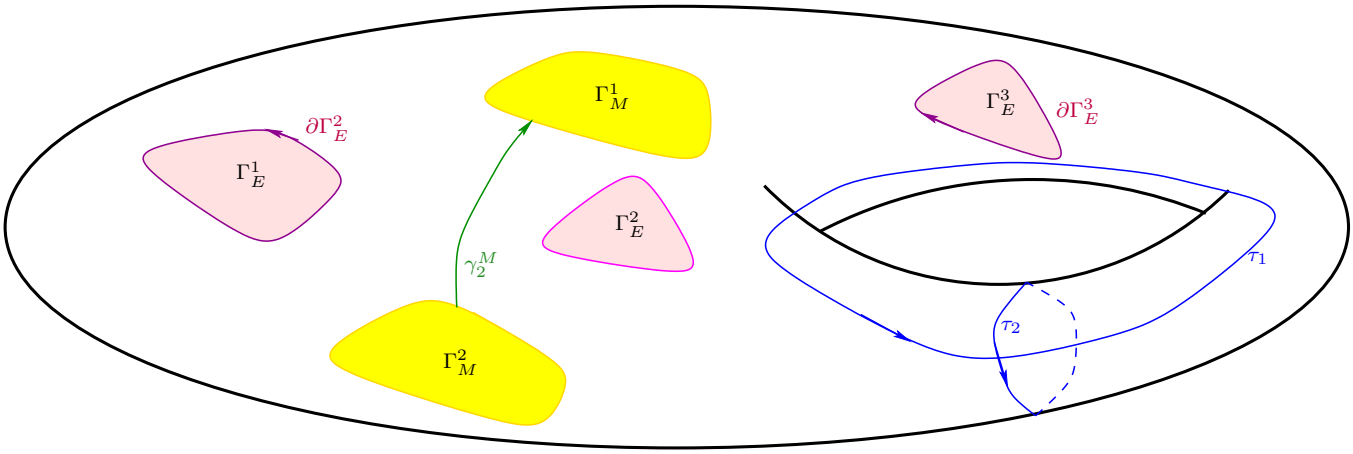

FIGURE 4 Torus-shaped Γ ($\beta_1(\Omega_C) = 1$); electric ports in pink, magnetic ports in yellow, $\boldsymbol{\Gamma_M}$**-relative** fundamental cycles in Γ_I are τ_1, τ_2 of class (T) colored blue, γ_2^M of class (CM) in green, $\partial\Gamma_E^2, \partial\Gamma_E^3$ of class (PM) in purple.

(CM) $N_M - 1$ directed curves $\gamma_2^M, \ldots, \gamma_{N_M}^M$ from Γ_M^1 to every other magnetic port ("magnetic connector cycles"),

(PM) the $N_E - 1$ boundaries $\partial\Gamma_E^k$, $k = 2, \ldots, N_E$, of the electric ports $\Gamma_E^2, \ldots, \Gamma_E^{N_E}$ ("electric port cycles").

Since $\partial\Gamma_I = \partial\Gamma_E \cup \partial\Gamma_M$, Poincaré-Lefschetz duality of homology theory guarantees that the Γ_E-relative fundamental cycles for $\mathcal{V}_E$ can be put in *duality* with the Γ_M-relative fundamental cycles for $\mathcal{V}_M$. This means that we can find finite sets of fundamental cycles of equal cardinality for both spaces and a bijective "pairing" between both sets that

- pairs the "topological" cycles of class (T) among themselves; these N_T cycles naturally come in pairs of dual cycles[3], *cf.* Assumption 3.
- pairs "connector cycles" of one set with "port cycles" of the other. Note that their numbers $N_E - 1$ and $N_M - 1$, respectively, agree.

Figure 5 and [1, Fig. 2] illustrate this relationship. The paired cycles can always be chosen to intersect transversally; they will be called *dual* to each other and the unique dual cycle of a given cycle will be tagged with $\widehat{\ }$. Then above statements can be expressed formally as

$$\widehat{\tau}_m = \tau_{N_T-m+1} \quad \Leftrightarrow \quad \tau_m = \widehat{\tau}_{N_T-m+1}\,, \qquad m = 1, \ldots, N_T\,, \tag{11a}$$

$$\widehat{\gamma}_k^E = \partial\Gamma_E^k \quad \Leftrightarrow \quad \gamma_k^E = \widehat{\partial\Gamma}_E^k\,, \qquad k = 2, \ldots, N_E\,, \tag{11b}$$

$$\widehat{\gamma}_\ell^M = \partial\Gamma_M^\ell \quad \Leftrightarrow \quad \gamma_\ell^M = \widehat{\partial\Gamma}_M^\ell\,, \qquad \ell = 2, \ldots, N_M\,. \tag{11c}$$

3.3 | Boundary scalar potentials

As we have seen in Theorem 1, tangential surface fields with vanishing $\mathbf{curl}_\Gamma/\mathrm{div}_\Gamma$ can be represented through surface scalar potentials plus contributions from low-dimensional co-homology spaces. First we focus on $\boldsymbol{\gamma_t}\mathcal{V}_E$ and the co-homology vectorfields associated with $\partial\Gamma_E$-relative non-bounding "electric connector cycles" of class (CE). Those co-homology vectorfields have a simple representation:

Let γ_k^E be a $\partial\Gamma_E$-relative fundamental cycle of class (CE) connecting Γ_E^1 and Γ_E^k, $k = 2, \ldots, N_E$. Then the associated tangential co-homology vectorfield $\mathbf{c} \in \mathcal{V}_E$ is given by[4]

$$\mathbf{c} := \mathbf{grad}_\Gamma\, \varphi_E^k \quad \text{with} \quad \varphi_E^k \in H^1(\Gamma)\,, \quad \varphi_E^k\big|_{\Gamma_E^k} \equiv 1\,, \quad \varphi_E^k\big|_{(\Gamma_E \cup \Gamma_M)\setminus\Gamma_E^k} \equiv 0\,. \tag{12}$$

That $\mathbf{c}$ satisfies condition (8), $\int_{\gamma_n^E} \mathbf{c}\cdot\mathrm{d}\mathbf{s} = \begin{cases} 1 & \text{for } n = k\,, \\ 0 & \text{else} \end{cases}$, is an immediate consequence of the fundamental theorem of calculus and the fact that the cycle γ_k^E connects the two electric ports Γ_E^k and Γ_E^1 with $\varphi_E^k\big|_{\Gamma_E^1} \equiv 0$. Moreover, let us write

[3] On a formal level the duality of (oriented) topological cycles can be expressed through their intersection numbers, see see [19, Sect. 6.4] and, in particular, Chapter 5 of [20].

[4] Our presentation relies on a few Sobolev spaces. Yet, their deeper mathematical properties will not be important here. For instance, the reader may just view $H^1(\Gamma)$ as "the space of continuous, piecewise differentiable scalar functions on Γ".

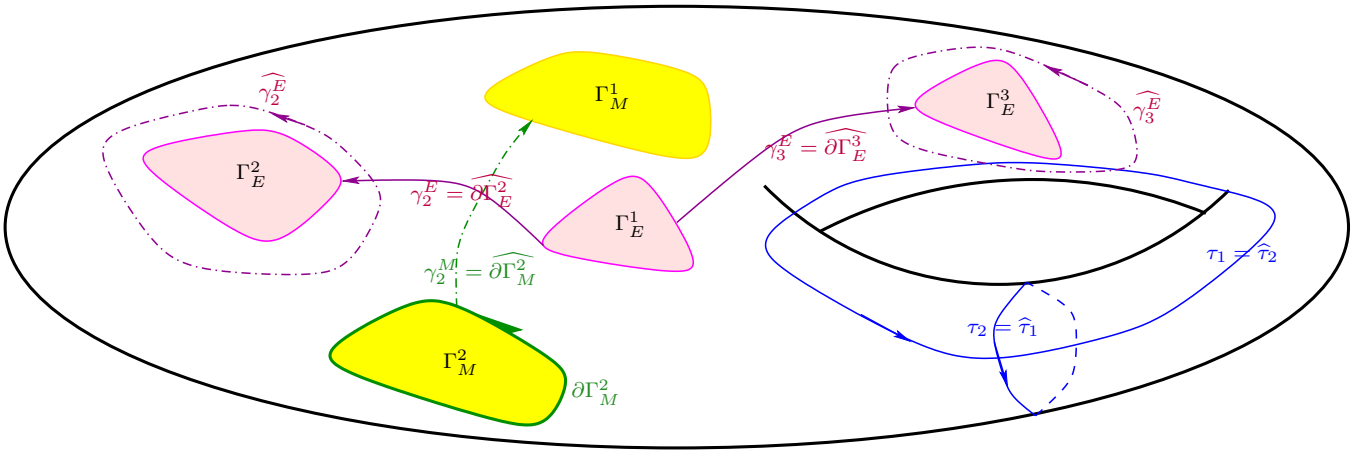

FIGURE 5 Torus-shaped Γ ($N_T = 2$, $N_E = 3$, $N_M = 2$): Γ_E-relative fundamental cycles for $\mathcal{V}_E$ as in Figure 3 are drawn with solid lines, their *dual* Γ_M-relative fundamental cycles are drawn with dashed lines and are marked with a $\widehat{\ }$. Study this figure alongside Figure 3 and Figure 4.

- $\mathbf{c}_2^E, \dots, \mathbf{c}_{N_M}^E \in \boldsymbol{H}(\mathrm{curl}_\Gamma, \Gamma) \cap \mathcal{V}_E$ for the $N_M - 1$ tangential co-homology vectorfields belonging to the Γ_E-relative non-bounding "magnetic port cycles" $\partial\Gamma_M^\ell$, $\ell = 2, \dots, N_M$, in Γ_I of class (PE),
- and $\mathbf{t}_1^E, \dots, \mathbf{t}_{N_T}^E \in \boldsymbol{H}(\mathrm{curl}_\Gamma, \Gamma) \cap \mathcal{V}_E$ for the tangential co-homology vectorfields corresponding to the "topological" Γ_E-relative non-bounding cycles $\tau_1, \dots, \tau_{N_T}$ in Γ_I of class (T). As will become clear in Section 3.4, those can be chosen to vanish on $\Gamma_M \cup \Gamma_E$.

These co-homology vectorfields will be examined more closely in Section 3.4. Now we are in a position to characterize the tangential trace space of $\mathcal{V}_E$ as

$$\begin{aligned} \boldsymbol{\gamma_t}\mathcal{V}_E &= \{\mathbf{m} \in \boldsymbol{H}^{-\frac{1}{2}}(\mathrm{curl}_\Gamma, \Gamma) : \ \mathbf{curl}_\Gamma \mathbf{m} = 0 \text{ on } \Gamma_I, \ \mathbf{m} = 0 \text{ on } \Gamma_E\} \\ &= \mathbf{grad}_\Gamma \mathcal{S}_E + \sum_{\ell=2}^{N_M} \mathrm{span}\{\mathbf{c}_\ell^E\} + \sum_{m=1}^{N_T} \mathrm{span}\{\mathbf{t}_m^E\} + \widetilde{\boldsymbol{H}}^{-\frac{1}{2}}(\mathrm{curl}_\Gamma, \Gamma_M) \ , \end{aligned} \tag{13}$$

with the space of scalar potentials

$$\mathcal{S}_E := \widetilde{H}^{\frac{1}{2}}_{\Gamma_E}(\Gamma) + \sum_{k=2}^{N_E} \mathrm{span}\{\varphi_E^k\} \ , \quad \widetilde{H}^{\frac{1}{2}}_{\Gamma_E}(\Gamma) := \{\psi \in H^{\frac{1}{2}}(\partial\Omega) : \ \psi|_{\Gamma_E} = 0\} \ , \tag{14}$$

and $\widetilde{\boldsymbol{H}}^{-\frac{1}{2}}(\mathrm{curl}_\Gamma, \Gamma_M)$ standing for the space of tangential traces supported in $\overline{\Gamma}_M$:

$$\widetilde{\boldsymbol{H}}^{-\frac{1}{2}}(\mathrm{curl}_\Gamma, \Gamma_M) := \{\mathbf{v} \in \boldsymbol{H}^{-\frac{1}{2}}(\mathrm{curl}_\Gamma, \Gamma) : \ \mathrm{supp}\, \mathbf{v} \subset \overline{\Gamma}_M\} \ . \tag{15}$$

An analogous representation holds for the magnetic space $\mathcal{V}_M$:

$$\begin{aligned} \boldsymbol{\gamma}_\times \mathcal{V}_M &= \{\mathbf{j} \in \boldsymbol{H}^{-\frac{1}{2}}(\mathrm{div}_\Gamma, \Gamma) : \ \mathrm{div}_\Gamma \mathbf{j} = 0 \text{ on } \Gamma_S, \ \mathbf{j} = 0 \text{ on } \Gamma_M\} \\ &= \mathbf{curl}_\Gamma \mathcal{S}_M + \sum_{k=2}^{N_E} \mathrm{span}\{\mathbf{c}_k^M\} + \sum_{m=1}^{N_T} \mathrm{span}\{\mathbf{t}_m^M\} + \widetilde{\boldsymbol{H}}^{-\frac{1}{2}}(\mathrm{div}_\Gamma, \Gamma_E) \ , \end{aligned} \tag{16}$$

with the scalar potential space given by

$$\mathcal{S}_M := \widetilde{H}^{\frac{1}{2}}_{\Gamma_M}(\Gamma) + \sum_{\ell=2}^{N_M} \mathrm{span}\{\varphi_M^\ell\} \ , \quad \widetilde{H}^{\frac{1}{2}}_{\Gamma_M}(\Gamma) := \{\psi \in H^{\frac{1}{2}}(\partial\Omega) : \ \psi|_{\Gamma_M} = 0\} \ , \tag{17}$$

and a space $\widetilde{\boldsymbol{H}}^{-\frac{1}{2}}(\mathrm{div}_\Gamma, \Gamma_E)$ defined in analogy to (15). The other building blocks correspond to those in (13):

- The functions $\varphi_M^\ell \in H^1(\Gamma)$, $\ell = 2, \dots, N_M$, are constant $\equiv 1$ on a single magnetic port Γ_M^ℓ and vanish on all other ports.
- The tangential co-homology vectorfields $\mathbf{c}_2^M, \dots, \mathbf{c}_{N_E}^M \in \boldsymbol{H}(\mathrm{div}_\Gamma, \Gamma) \cap \mathcal{V}_M$ belong to the Γ_M-relative non-bounding boundaries $\partial\Gamma_E^k$, $k = 2, \dots, N_E$.
- The functions $\mathbf{t}_M^m$, $m = 1, \dots, N_T$ are $\frac{\pi}{2}$-rotated versions of $\mathbf{t}_E^m$.

3.4 | Construction of tangential co-homology vectorfields

Having settled the case of scalar potentials, we focus on the co-homology vectorfields $\mathbf{c}_2^E, \ldots, \mathbf{c}_{N_M}^E$ and $\mathbf{t}_1^E, \ldots, \mathbf{t}_{N_T}^E$. Their construction obeys an common principle. Each one of them is associated with a Γ_E-relative non-bounding cycle $\partial\Gamma_M^2, \ldots, \partial\Gamma_M^{N_M}$ of class (PE) or $\tau_1, \ldots, \tau_{N_T}$ of class (T), respectively, as we have learned in Section 3.2. There we also identified their *dual cycles* $\gamma_\ell^M = \widehat{\partial\Gamma_M^\ell}$, $\ell = 2, \ldots, N_M$, and $\widehat{\tau_m} = \tau_{N_T - m + 1}$, $m = 1, \ldots, N_T$, see Figure 4.

Dual cycles, also called "cuts" in this context, are key ingredients for our construction. Write $\mathbf{c}^E \in \{\mathbf{c}_2^E, \ldots, \mathbf{c}_{N_M}^E, \mathbf{t}_1^E, \ldots, \mathbf{t}_{N_T}^E\}$ for a generic tangential co-homology vectorfield in $\mathcal{V}_E$, γ for its associated $\partial\Gamma_E$-relative fundamental cycle, and $\widehat{\gamma} \subset \Gamma_I$ for the corresponding dual cycle. Then we can set

$$\mathbf{c}^E := \begin{cases} \widetilde{\mathbf{grad}_\Gamma}\,\psi^E \text{ on } \Gamma \setminus \Gamma_M\,, \\ \text{any extension on } \Gamma_M\,, \end{cases} \quad \text{with} \quad \begin{aligned} &\psi^E \in H^1(\Gamma \setminus (\Gamma_M \cup \widehat{\gamma}))\,, \\ &\psi^E = 0 \text{ on } \Gamma_E\,, \\ &[\![\psi^E]\!]_{\widehat{\gamma}} = 1\,, \end{aligned} \tag{18}$$

where $[\![\psi]\!]_{\widehat{\gamma}}$ denotes the jump of a function across the oriented curve $\widehat{\gamma}$ and $\widetilde{\mathbf{grad}_\Gamma}$ is the (piecewise) surface gradient on $\Gamma \setminus \widehat{\gamma}$. We have enough flexibility in choosing ψ^E to ensure that $\operatorname{supp} \mathbf{c}^E$ is inside a neighborhood of $\widehat{\gamma}$.

We skip the details of the construction of the co-homology vectorfields $\mathbf{c}_k^M \in \boldsymbol{H}^{-\frac{1}{2}}(\mathrm{div}_\Gamma, \Gamma)$, $k = 2, \ldots, N_E$, for $\mathcal{V}_M$, which follows similar lines and just involves a role reversal of Γ_M and Γ_E, and replacing N_M with N_E and $\mathbf{grad}_\Gamma$ with $\mathbf{curl}_\Gamma$, *cf.* Remark 2

4 | VARIATIONAL FORMULATIONS

The evolution of the electric field $\mathbf{E} = \mathbf{E}(\boldsymbol{x}, t)$ and of the magnetic field $\mathbf{H} = \mathbf{H}(\boldsymbol{x}, t)$ in Ω is governed by the transient Maxwell's equations:

$$\partial_t(\epsilon\mathbf{E}) \quad + \quad \sigma\mathbf{E} \quad - \mathbf{curl}\,\mathbf{H} = 0\,, \tag{AL}$$

$$\partial_t(\mu\mathbf{H}) \quad + \quad \mathbf{curl}\,\mathbf{E} \quad = 0\,. \tag{FL}$$

with uniformly positive, possibly spatially varying material coefficients $\epsilon = \epsilon(\boldsymbol{x})$ and $\mu = \mu(\boldsymbol{x})$, and $\sigma = \sigma(\boldsymbol{x}) \geq 0$. These partial differential equations can be cast in weak form in two different ways. In both cases we take for granted that $\mathbf{E}(t) \in \mathcal{V}_E$ and $\mathbf{H}(t) \in \mathcal{V}_M$ for all times.

4.1 | E-based weak formulation

We test Ampere's law (AL) with $\mathbf{E}' \in \mathcal{V}_E$, integrate over Ω and then integrate by parts by (1), which yields

$$\int_\Omega \big(\partial_t(\epsilon\mathbf{E}) + \sigma\mathbf{E}\big) \cdot \mathbf{E}' - \mathbf{H} \cdot \mathbf{curl}\,\mathbf{E}'\,\mathrm{d}\boldsymbol{x} - \int_\Gamma \boldsymbol{\gamma}_\times\mathbf{H} \cdot \boldsymbol{\gamma}_t\mathbf{E}'\,\mathrm{d}S = 0 \quad \forall \mathbf{E}' \in \mathcal{V}_E\,. \tag{19}$$

Appealing to (16) and (13), we can write for the tangential trace of any $\mathbf{E}' \in \mathcal{V}_E$

$$\boldsymbol{\gamma}_t\mathbf{E}' = \mathbf{grad}_\Gamma\,\varphi_E' + \sum_{\ell=2}^{N_M} \alpha_\ell \mathbf{c}_\ell^E + \sum_{m=1}^{N_T} \beta_m \mathbf{t}_m^E + \widetilde{\mathbf{m}}' \quad \text{on} \quad \Gamma\,; \tag{20}$$

with $\varphi_E' \in \mathcal{S}_E$, $\alpha_\ell, \beta_m \in \mathbb{R}$, $\widetilde{\mathbf{m}}' \in \widetilde{\boldsymbol{H}}^{-\frac{1}{2}}(\mathrm{curl}_\Gamma, \Gamma_M)$, see (15).

We examine the boundary term in (19) and start with the observation that the integrand vanishes on $\Gamma_M \cup \Gamma_E$ so that we can confine integration to Γ_I. Then we plug in the representation (20), note that the contribution $\widetilde{\mathbf{m}}'$ does not matter, and get

$$\int_{\Gamma_I} \boldsymbol{\gamma}_\times\mathbf{H} \cdot \boldsymbol{\gamma}_t\mathbf{E}'\,\mathrm{d}S = \int_{\Gamma_I} \boldsymbol{\gamma}_\times\mathbf{H} \cdot \big(\mathbf{grad}_\Gamma\,\varphi_E' + \sum_{\ell=2}^{N_M} \alpha_\ell \mathbf{c}_\ell^E + \sum_{m=1}^{N_T} \beta_m \mathbf{t}_m^E\big)\,.$$

Next, embarking on "formal computations", we use the integration by parts formula

$$\int_{\Gamma_I} \mathbf{v} \cdot \mathbf{grad}_\Gamma\,\psi\,\mathrm{d}S = -\int_{\Gamma_I} \psi\,\mathrm{div}_\Gamma\mathbf{v}\,\mathrm{d}S + \int_{\partial\Gamma_I} \psi\,(\boldsymbol{n} \times \mathbf{v}) \cdot \mathrm{d}s \tag{21}$$

for all $\psi \in H^{\frac{1}{2}}(\Gamma_I)$, $\mathbf{v} \in \boldsymbol{H}^{-\frac{1}{2}}(\mathrm{div}_\Gamma, \Gamma_I)$, which yields a sum of circulation integrals

$$\int_{\Gamma_I} \boldsymbol{\gamma}_\times\mathbf{H} \cdot \mathbf{grad}_\Gamma\,\varphi_E'\,\mathrm{d}S = -\int_{\Gamma_I} \varphi_E' \underbrace{\mathrm{div}_\Gamma(\boldsymbol{\gamma}_\times\mathbf{H})}_{=0}\,\mathrm{d}S + \int_{\partial\Gamma_E} \varphi_E'\,\mathbf{H} \cdot \mathrm{d}s = \sum_{k=1}^{N_E} \varphi_E'|_{\Gamma_E^k} \int_{\partial\Gamma_E^k} \mathbf{H} \cdot \mathrm{d}s\,. \tag{22}$$

Again, we use integration by parts according to (21) to deal with the contribution of the co-homology vectorfields $\mathbf{c}_\ell^E$ and $\mathbf{t}_m^E$. Parallel to the construction in Section 3.4, we consider a generic co-homology vectorfield $\mathbf{c}^E$ given by the formula from (18). Refer to that formula for notations.

$$\begin{aligned}\int_{\Gamma_I} \boldsymbol{\gamma}_\times \mathbf{H} \cdot \mathbf{c}^E \,\mathrm{d}S &= \int_{\Gamma_I} \boldsymbol{\gamma}_\times \mathbf{H} \cdot \widetilde{\mathbf{grad}_\Gamma \psi^E} \,\mathrm{d}S = -\int_{\Gamma_I} \underbrace{\mathrm{div}_\Gamma \boldsymbol{\gamma}_\times \mathbf{H}}_{=0} \, \psi^E \,\mathrm{d}S + \int_{\partial(\Gamma_I \setminus \widehat{\gamma})} \psi^E \, \boldsymbol{\gamma_t} \mathbf{H} \cdot \mathrm{d}s \\ &\overset{(*)}{=} \int_{\widehat{\gamma}} \left[\!\left[\psi^E \right]\!\right]_{\widehat{\gamma}} \boldsymbol{\gamma_t} \mathbf{H} \cdot \mathrm{d}s = \int_{\widehat{\gamma}} \boldsymbol{\gamma_t} \mathbf{H} \cdot \mathrm{d}s \,,\end{aligned} \tag{23}$$

because $\psi^E \boldsymbol{\gamma_t} \mathbf{H}$ has vanishing tangential component on both $\partial\Gamma_E$ and $\partial\Gamma_M$. We point out that integration in $\int_{\partial(\Gamma_I \setminus \widehat{\gamma})} \ldots$ visits both sides of $\widehat{\gamma}$ which accounts for the emergence of the jump in step $(*)$.

Faraday's law (FL) is kept in "strong form" and just tested with $\mathbf{H}' \in \mathcal{V}_M$. This results in the final $\mathbf{E}$-based spatial variational formulation: seek $\mathbf{E} : [0,T] \to \mathcal{V}_E$, $\mathbf{H} : [0,T] \to \mathcal{V}_M$, such that

$$\begin{aligned}&\int_\Omega \big(\partial_t(\epsilon \mathbf{E}) + \sigma \mathbf{E}\big) \cdot \mathbf{E}' - \mathbf{H} \cdot \mathbf{curl}\, \mathbf{E}' \,\mathrm{d}\boldsymbol{x} - \sum_{k=2}^{N_E} \varphi'_E\big|_{\Gamma_E^k} \int_{\partial\Gamma_E^k} \mathbf{H} \cdot \mathrm{d}s - \sum_{\ell=2}^{N_M} \alpha_\ell \int_{\gamma_\ell^M} \boldsymbol{\gamma_t} \mathbf{H} \cdot \mathrm{d}s - \sum_{m=1}^{N_T} \beta_m \int_{\widehat{\tau}_m} \boldsymbol{\gamma_t} \mathbf{H} \cdot \mathrm{d}s \quad = 0 \,, \\ &\int_\Omega \big(\partial_t(\mu \mathbf{H}) + \mathbf{curl}\, \mathbf{E}\big) \cdot \mathbf{H}' \,\mathrm{d}\boldsymbol{x} \quad = 0\end{aligned} \tag{24}$$

for all $\mathbf{E}' \in \mathcal{V}_E$ with $\boldsymbol{\gamma_t} \mathbf{E}'$ according to (20), and for all $\mathbf{H}' \in \mathcal{V}_M$. We point out that the dualities (11) have been used to rewrite the circulation integrals.

4.2 | $\mathbf{H}$-based variational formulation

Now, we test Faraday's law (FL) with $\mathbf{H}' \in \mathcal{V}_M$ and, after integration by parts, arrive at

$$\int_\Omega \partial_t(\mu \mathbf{H}) \cdot \mathbf{H}' + \mathbf{E} \cdot \mathbf{curl}\, \mathbf{H}' \,\mathrm{d}\boldsymbol{x} - \int_\Gamma \boldsymbol{\gamma_t} \mathbf{E} \cdot \boldsymbol{\gamma}_\times \mathbf{H}' \,\mathrm{d}S = 0 \quad \forall \mathbf{H}' \in \mathcal{V}_M \,. \tag{25}$$

For the rotated tangential trace of the test field we use the representation from (16):

$$\boldsymbol{\gamma}_\times \mathbf{H}' = \mathbf{curl}_\Gamma \varphi'_M + \sum_{k=2}^{N_E} \alpha_k \mathbf{c}_k^M + \sum_{m=1}^{N_T} \beta_m \mathbf{t}_m^M + \widetilde{\mathbf{j}}' \quad \text{on} \quad \Gamma \,, \tag{26}$$

where $\varphi'_M \in \mathcal{S}_M$, $\alpha_k, \beta_m \in \mathbb{R}$, and $\widetilde{\mathbf{j}} \in \widetilde{\boldsymbol{H}}^{-\frac{1}{2}}(\mathrm{div}_\Gamma, \Gamma_E)$. Parallel to the developments of Section 4.1 we can convert the boundary terms into

$$\int_\Gamma \boldsymbol{\gamma_t} \mathbf{E} \cdot \mathbf{curl}_\Gamma \varphi'_M \,\mathrm{d}S = \sum_{\ell=1}^{N_M} \varphi'_M\big|_{\Gamma_M^\ell} \int_{\partial\Gamma_M^\ell} \mathbf{E} \cdot \mathrm{d}s \,, \quad \int_\Gamma \boldsymbol{\gamma_t} \mathbf{E} \cdot \mathbf{c}_k^M \,\mathrm{d}S = \int_{\partial\Gamma_E^k} \boldsymbol{\gamma_t} \mathbf{E} \cdot \mathrm{d}s \,, \quad \int_\Gamma \boldsymbol{\gamma_t} \mathbf{E} \cdot \mathbf{t}_m^M \,\mathrm{d}S = \int_{\widehat{\tau}_m} \boldsymbol{\gamma_t} \mathbf{E} \cdot \mathrm{d}s \,. \tag{27}$$

This yields the so-called $\mathbf{H}$-based variational formulation, which involves Ampere's law (AL) in strong form: seek $\mathbf{E} : [0,T] \to \mathcal{V}_E$ and $\mathbf{H} : [0,T] \to \mathcal{V}_M$ such that

$$\begin{aligned}&\int_\Omega \big(\partial_t(\epsilon \mathbf{E}) + \sigma \mathbf{E}\big) \cdot \mathbf{E}' - \mathbf{curl}\, \mathbf{H} \cdot \mathbf{E}' \,\mathrm{d}\boldsymbol{x} \quad = 0 \,, \\ &\int_\Omega \partial_t(\mu \mathbf{H}) \cdot \mathbf{H}' + \mathbf{E} \cdot \mathbf{curl}\, \mathbf{H}' \,\mathrm{d}\boldsymbol{x} - \sum_{\ell=1}^{N_M} \varphi'_M\big|_{\Gamma_M^\ell} \int_{\partial\Gamma_M^\ell} \mathbf{E} \cdot \mathrm{d}s - \sum_{k=2}^{N_E} \alpha_k \int_{\partial\Gamma_E^k} \boldsymbol{\gamma_t} \mathbf{E} \cdot \mathrm{d}s - \sum_{m=1}^{N_T} \beta_m \int_{\widehat{\tau}_m} \boldsymbol{\gamma_t} \mathbf{E} \cdot \mathrm{d}s \quad = 0 \,,\end{aligned} \tag{28}$$

for all $\mathbf{E}' \in \mathcal{V}_E$ and $\mathbf{H}' \in \mathcal{V}_M$. For the latter we have plugged in the representation (26) of $\boldsymbol{\gamma}_\times \mathbf{H}'$.

Remark 5. If $\Gamma_R \neq \emptyset$, the impedance boundary conditions give rise to extra terms

$$\int_{\Gamma_R} \big(\mathsf{Z}^{-1}(\boldsymbol{\gamma_t} \mathbf{E})\big)(t) \cdot \boldsymbol{\gamma_t} \mathbf{E}' \,\mathrm{d}S \quad \text{and} \quad \int_{\Gamma_R} \big(\mathsf{Z}(\boldsymbol{\gamma}_\times \mathbf{H})\big)(t) \cdot \boldsymbol{\gamma_t} \mathbf{H}' \,\mathrm{d}S \tag{29}$$

entering the first equation of (24) and (28), respectively.

5 | PORT CONDITIONS

The electric and magnetic time-dependent port quantities in circuit models are

- The **electric potentials** $U_k = U_k(t)$ at the electric ports Γ_E^k, $k = 2, \ldots, N_E$, Γ_E^1 assumed to be grounded.
- The **electric currents** $J_k = J_K(t)$ at the electric ports Γ_E^k, $k = 1, \ldots, N_E$. Their sum is zero.
- The **magnetomotive forces** (M.M.F.) $F_\ell = F_\ell(t)$ at the magnetic ports Γ_M^ℓ, $\ell = 2, \ldots, N_M$, Γ_M^1 as reference.

- The **magnetic fluxes** $\dot{B}_\ell = \dot{B}_\ell(t)$ at the magnetic ports, $\ell = 2, \ldots, N_M$. Those add to zero.
- The **linked magnetic fluxes** $\dot{B}^T_m = \dot{B}_m(t)$, $m = 1, \ldots, N_T$, for loops of the circuit domain Ω_C.
- The **linked electric currents** $J^T_m = J^T_m(t)$, $m = 1, \ldots, N_T$, associated with loops of Ω_C, too.

We hark back to the representations of tangential traces:

$$\text{(13)} \quad \Rightarrow \qquad \boldsymbol{\gamma_t}\mathbf{E}(t) = \mathbf{grad}_\Gamma \varphi_E(t) + \sum_{\ell=2}^{N_M} \alpha^E_\ell(t)\mathbf{c}^E_\ell + \sum_{m=1}^{N_T} \beta^E_m(t)\mathbf{t}^E_m + \widetilde{\mathbf{m}}(t)\ , \quad \varphi_E \in \mathcal{S}_E\,; \tag{30}$$

$$\text{(16)} \quad \Rightarrow \qquad \boldsymbol{\gamma}_\times \mathbf{H}(t) = \mathbf{curl}_\Gamma \varphi_M(t) + \sum_{k=2}^{N_E} \alpha^M_k(t)\mathbf{c}^M_k + \sum_{m=1}^{N_T} \beta^M_m(t)\mathbf{t}^M_m + \widetilde{\mathbf{j}}(t)\ , \quad \varphi_M \in \mathcal{S}_M\ . \tag{31}$$

From them and Maxwell's equations we extract a comprehensive set of expressions for the port quantities, for

$$\text{electric port potentials:} \qquad U_k(t) = \varphi_E(t)|_{\Gamma^k_E} = \int_{\widehat{\gamma}^M_k = \gamma^E_k} \mathbf{E}(t)\cdot \mathrm{d}s\ , \tag{32a}$$

$$\text{electric port currents:} \qquad J_k(t) = \alpha^M_k(t) = \int_{\partial\Gamma^k_E} \mathbf{H}(t)\cdot \mathrm{d}s\ , \tag{32b}$$

$$\text{port M.M.F.:} \qquad F_\ell(t) = \varphi_M(t)|_{\Gamma^M_\ell} = \int_{\widehat{\gamma}^E_\ell = \gamma^\ell_M} \mathbf{H}(t)\cdot \mathrm{d}s\ , \tag{32c}$$

$$\text{port magnetic fluxes:} \qquad \dot{B}_\ell(t) = \alpha^E_\ell(t) = \int_{\partial\Gamma^\ell_M} \mathbf{E}(t)\cdot \mathrm{d}s\ , \tag{32d}$$

$$\text{linked magnetic fluxes:} \qquad \dot{B}^T_m(t) = \beta^E_m(t) = \int_{\widehat{\tau}_m} \mathbf{E}(t)\cdot \mathrm{d}s\ , \tag{32e}$$

$$\text{linked electric currents:} \qquad J^T_m(t) = \beta^M_m(t) = \int_{\widehat{\tau}_m} \mathbf{H}(t)\cdot \mathrm{d}s\ , \tag{32f}$$

for all $k = 2, \ldots, N_E$, $\ell = 2, \ldots, N_M$, $m = 1, \ldots, N_T$. The formulas in the middle column we may call *essential port conditions*, because they are directly imposed on the fields through (30) and (31), whereas the formulas in the right column may be called *weak port conditions*, because they permit us to enforce them through terms in the variational formulations.

Remark 6. For the port quantities (32) the indices k and ℓ run from 2. Don't we neglect fluxes, thus? No, because owing to $\operatorname{div}\mathbf{curl}\,\mathbf{H} = \operatorname{div}\mathbf{curl}\,\mathbf{E} = 0$, and the boundary conditions inherent in $\mathcal{V}_E/\mathcal{V}_M$ we find the flux balance laws

$$\sum_{k=1}^{N_E} J_k(t) = \sum_{k=1}^{N_E} \int_{\partial\Gamma^k_E} \mathbf{H}(t)\cdot \mathrm{d}s = 0 \quad , \quad \sum_{\ell=1}^{N_M} \dot{B}_\ell(t) = \sum_{\ell=1}^{N_M} \int_{\partial\Gamma^\ell_M} \mathbf{E}(t)\cdot \mathrm{d}s = 0\ , \tag{33}$$

which makes it possible to recover the "missing flux" from the others.

In order to endow port conditions with their "natural meaning" in circuit theory we have to impose constraints on the cycles:

(I) The concept of generic port voltages and port M.M.F.s entails the existence of global electric and magnetic scalar potentials, which, however, cannot be reconciled with non-zero linked fluxed given as circulations along topological cycles τ_m, $m-1, \ldots, N_T$. This difficulty can be resolved by treating the tological cycles as "cuts", which render $\Gamma \setminus \bigcup_m \tau_m$ topologically trivial. Therefore, once we restrict all connector cycles to that complement, path integrals along them define meaningful voltages/M.M.F.s.

Assumption 2. None of the connector cycles $\gamma^E_1, \ldots, \gamma^E_{N_E}$ and $\gamma^M_1, \ldots, \gamma^M_{N_M}$ intersects any of the topological cycles $\tau_1, \ldots, \tau_{N_T}$.

We can always find connector cycles with this property, because $\Gamma \setminus \bigcup_m \tau_m$ is still connected. The arrangements displayed in Figure 3 and Figure 4 comply with Assumption 2, and another illustration is given in Figure 6.

The reader must be aware that in the case $N_T > 0$ the choice of the connector cycle is a modeling decision, which will have a big impact on the resulting electromagnetic fields; simulation results covered in Section 7 will demonstrate this.

(II) We have already taken for granted that the "topological cycles" τ_m, $m = 1, \ldots, N_T$, come in dual pairs, recall Section 3.2. They are needed to define the linked fluxes $\dot{B}^T_m$ and currents J^T_m as non-local coupling quantities in (32e) and (32f). In order to give these quantities their "natural meaning", we have to make the following assumption, see Figure 6 for an illustration. For an in-depth discussion of this classification of topological cycles refer to [21].

Assumption 3. Half of the cycles τ_m are bounding with respect to Ω_C, whereas their duals are bounding with respect to Ω.

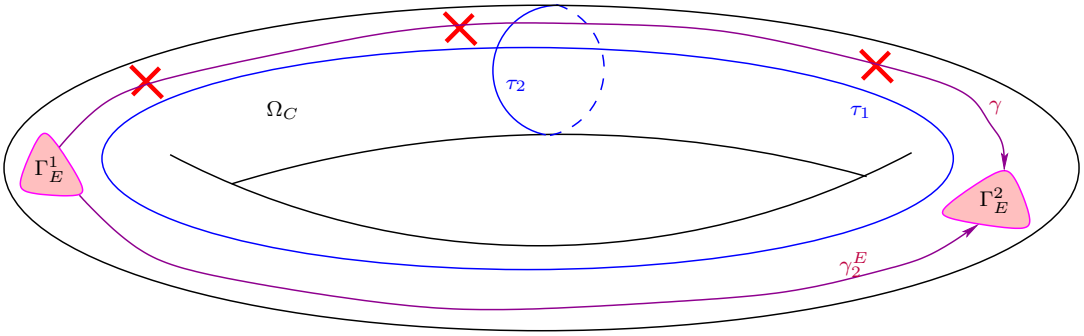

FIGURE 6 Torus-shaped Ω_C with two electric ports, $N_T = 2$, $N_E = 2$: The connector cycle γ_2^E stays clear of the topological cycles and fulfills Assumption 2, whereas γ is not admissible given how τ_2 is chosen. Note that the topological cycles comply with Assumption 3: τ_2 is bounding with respect to Ω_C, τ_1 bounds with respect to $\Omega := \mathbb{R}^3 \setminus \Omega_C$.

In fact, this "assumption" could also have been labeled a proposition, because we can always obtain the topological cycles as boundaries of $N_T/2$ "cuts" in Ω_C and Ω, respectively [22, 20, 23]. In [24] it was established that these cuts can be chosen so that they come in pairs whose boundaries constitute dual topological cycles.

Summing up, Assumption 3 will permit us to view $\dot{B}_m^T$ as the electromotive force around a loop of Ω_C and J_m^T as the current flowing in a section of it. For instance, in the situation depicted in Figure 6 $\dot{B}_2^T$ is the variation of the magnetic flux through the central tunnel, whereas J_2^T stands for a current flowing through it.

5.1 | Ports in E-based Model (24)

In light of the definition (2) of $\mathcal{V}_E$ and (30) we write the time-dependent electric field $\mathbf{E} = \mathbf{E}(t)$ as direct sum (Colors indicate the related cycle classes as in Section 3.2.)

$$\mathbf{E}(t) \quad = \quad \mathbf{E}_0(t) \quad + \quad \mathbf{grad}(\mathsf{X}\rho_E(t)) \quad + \quad \sum_{k=2}^{N_E} U_k(t)\,\mathbf{grad}\,\mathsf{X}\nu_E^k \quad + \quad \sum_{\ell=2}^{N_M} \dot{B}_\ell(t)\mathbf{C}_\ell^E \quad + \quad \sum_{m=1}^{N_T} \dot{B}_m^T(t)\mathbf{T}_m^E \qquad , \tag{34}$$

where

- $\mathbf{E}_0(t) \in \boldsymbol{H}_{\Gamma\setminus\Gamma_M}(\mathbf{curl},\Omega) := \{\mathbf{V} \in \boldsymbol{H}(\mathbf{curl},\Omega) : \boldsymbol{\gamma_t}\mathbf{V} = 0 \text{ on } \Gamma \setminus \Gamma_M\}$ is the electric field in the interior of the field domain Ω,
- $\rho_E(t) \in \widetilde{H}^{1/2}_{\Gamma_E}(\Gamma_I) := \{\psi \in H^{\frac{1}{2}}(\Gamma_I \cup \Gamma_E) : \psi = 0 \text{ on } \Gamma_E\}$ is the scalar surface potential on the insulating parts of the boundary,
- $\mathsf{X} : H^{\frac{1}{2}}(\Gamma_I \cup \Gamma_E) \to H^1(\Omega)$ is a continuous extension operator, mapping functions on $\Gamma_I \cup \Gamma_E$ to functions defined on Ω,
- $\nu_E^k \in H^{\frac{1}{2}}(\partial\Omega)$ satisfies $\nu_E^k\big|_{\Gamma_E^k} \equiv 1$, $\nu_E^k\big|_{\Gamma_E^m} = 0$ for $m \neq k$, that is, the function ν_E^k attains the value 1 on the electric port Γ_E^k, is "continuous", and vanishes on all other ports,
- $\mathbf{C}_\ell^E \in \boldsymbol{H}(\mathbf{curl},\Omega)$, is an extension of the co-homology tangential surface vectorfield $\mathbf{c}_\ell^E$ into Ω, $\ell = 2,\ldots,N_M$: $\boldsymbol{\gamma_t}\mathbf{C}_\ell^E = \mathbf{c}_\ell^E$,
- $\mathbf{T}_m^E \in \boldsymbol{H}(\mathbf{curl},\Omega)$ extends $\mathbf{t}_m^E$: $\boldsymbol{\gamma_t}\mathbf{T}_m^E = \mathbf{t}_m^E$, $m = 1,\ldots,N_T$.

Next, we use the "weak expressions" from the right column of (32) for the port currents J_k from (32b), for the magnetomotive forces F_ℓ from (32c), and for the linked currents from (32f) to replace the three path integrals in (24) with associated port quantities:

$$\int_{\partial\Gamma_E^k} \mathbf{H}\cdot\mathrm{d}s \;\longrightarrow\; J_k\,, \quad \int_{\widehat{\gamma}_\ell^E} \boldsymbol{\gamma_t}\mathbf{H}\cdot\mathrm{d}s \;\longrightarrow\; F_\ell\,, \quad \int_{\widehat{\tau}_m} \boldsymbol{\gamma_t}\mathbf{H}\cdot\mathrm{d}s \;\longrightarrow\; J_m^T\,. \tag{35}$$

Another change compared to (24) is that we relax the smoothness requirements for the magnetic field to $\mathbf{H}(t) \in \boldsymbol{L}^2(\Omega)$ and also allow $\mathbf{H}' \in \boldsymbol{L}^2(\Omega)$, because no extra regularity is required to render the variational formulation well-defined.

As already done in the derivation of (24), the splitting (34) is also applied to the test field $\mathbf{E}'$, and this yields

(i) two variational equations corresponding to testing with $\mathbf{E}_0' \in \boldsymbol{H}_{\Gamma\setminus\Gamma_M}(\mathbf{curl},\Omega)$ and $\mathsf{X}\rho_E' \in \widetilde{H}^{1/2}_{\Gamma_E}(\Gamma_I)$, yielding (36a) and (36b) below,

(ii) and, from (10), $N := N_T + \max\{N_M, 1\} + \max\{N_E, 1\} - 2$ equations from testing with $\mathbf{grad}\,\mathsf{X}\nu_E^k$, $\mathbf{C}_\ell^E$, and $\mathbf{T}_m^E$, $k = 2, \dots, N_E$, $\ell = 2, \dots, N_M$, $m = 1, \dots, N_T$, resulting in (36c)–(36e) below.

Eventually, we end up with the variational problem:

Seek $\mathbf{E}_0 : [0,T] \to \boldsymbol{H}_{\Gamma\setminus\Gamma_M}(\mathbf{curl}, \Omega)$, $\rho_E : [0,T] \to \widetilde{H}^{1/2}_{\Gamma_E}(\Gamma_I)$, $U_k : [0,T] \to \mathbb{R}$, $\dot{B}_\ell : [0,T] \to \mathbb{R}$, $U_k; [0,T] \to \mathbb{R}$, $F_\ell : [0,T] \to \mathbb{R}$, $\dot{B}_m^T : [0,T] \to \mathbb{R}$, $\mathbf{H} : [0,T] \to \boldsymbol{L}^2(\Omega)$ such that

$$\int_\Omega \big(\partial_t(\epsilon\mathbf{E})(t) + \sigma\mathbf{E}(t)\big) \cdot \mathbf{E}_0' - \mathbf{H}(t) \cdot \mathbf{curl}\,\mathbf{E}_0' \,\mathrm{d}\boldsymbol{x} \qquad = 0\,, \tag{36a}$$

$$\int_\Omega \big(\partial_t(\epsilon\mathbf{E})(t) + \sigma\mathbf{E}(t)\big) \cdot \mathbf{grad}\,\mathsf{X}\rho_E' \,\mathrm{d}\boldsymbol{x} \qquad = 0\,, \tag{36b}$$

$$\int_\Omega \big(\partial_t(\epsilon\mathbf{E})(t) + \sigma\mathbf{E}(t)\big) \cdot \mathbf{grad}\,\mathsf{X}\nu_E^k \,\mathrm{d}\boldsymbol{x} \quad - J_k(t) = 0\,, \tag{36c}$$

$$\int_\Omega \big(\partial_t(\epsilon\mathbf{E})(t) + \sigma\mathbf{E}(t)\big) \cdot \mathbf{C}_\ell^E - \mathbf{H}(t) \cdot \mathbf{curl}\,\mathbf{C}_\ell^E \,\mathrm{d}\boldsymbol{x} \quad - F_\ell(t) = 0\,, \tag{36d}$$

$$\int_\Omega \big(\partial_t(\epsilon\mathbf{E})(t) + \sigma\mathbf{E}(t)\big) \cdot \mathbf{T}_m^E - \mathbf{H}(t) \cdot \mathbf{curl}\,\mathbf{T}_m^E \,\mathrm{d}\boldsymbol{x} \quad - J_m^T(t) = 0\,, \tag{36e}$$

$$\int_\Omega \big(\partial_t(\mu\mathbf{H})(t) + \mathbf{curl}\,\mathbf{E}(t)\big) \cdot \mathbf{H}' \,\mathrm{d}\boldsymbol{x} \qquad = 0 \tag{36f}$$

for all $\mathbf{E}_0' \in \boldsymbol{H}_{\Gamma\setminus\Gamma_M}(\mathbf{curl}, \Omega)$, $\rho_E' \in \widetilde{H}^{1/2}_{\Gamma_E}(\Gamma_I)$, $k = 2, \dots, N_E$, $\ell = 2, \dots, N_M$, $m = 1, \dots, N_T$, and $\mathbf{H}' \in \boldsymbol{L}^2(\Omega)$.

Note that in (36) $\mathbf{E}$ has to be read as an expression depending affine-linearly on $\mathbf{E}_0$, ρ_E, U_k,$\dot{B}_\ell$, and $\dot{B}_m^T$ according to (34).

Formally, there is a mismatch of the number of equations and unknowns in (36) ("Six equations for nine unknowns"), which leaves freedom to imposed values for port quantities or relationships between them. This is how we can introduce sources and circuit relations into the model.

Remark 7. Elimination of magnetic field. Assume that none of the material coefficients ϵ, σ, and μ depends on time. Then we can

1. differentiate (36a)–(36e) with respect to time t, which amounts to replacing
$$\partial(\epsilon\mathbf{E})(t) \to \epsilon\partial_t^2\mathbf{E}(t)\,, \quad \sigma\mathbf{E}(t) \to \sigma\partial_t\mathbf{E}(t)\,, \quad \mathbf{H}(t) \to \partial_t\mathbf{H}(t)\,.$$
2. move ∂_t right in front of $\mathbf{H}$ in (36f): $\partial_t(\mu\mathbf{H})(t) \to \mu\partial_t\mathbf{H}$.

Subsequently, we can test (36f) with $\mu^{-1}\,\mathbf{curl}\,\mathbf{E}_0'$, $\mu^{-1}\,\mathbf{curl}\,\mathbf{C}_\ell^E$, and $\mu^{-1}\,\mathbf{curl}\,\mathbf{T}_m^E$, respectively, and use the resulting equation to eliminate $\mathbf{H}(t)$ in (36a), (36d), and (36e). We end up with an evolution equation for the electric field $\mathbf{E} = \mathbf{E}(t)$ alone, second-order in time, which still contains all the port quantities.

5.2 | Ports in H-Based Model (28)

Of course, the approach to (28) runs parallel to the developments of Section 5.1. From (3)/(31) we get the direct-sum representation

$$\mathbf{H}(t) = \mathbf{H}_0(t) + \mathbf{grad}\,\mathsf{X}\rho_M(t) + \sum_{\ell=2}^{N_M} F_\ell(t)\,\mathbf{grad}\,\mathsf{X}\nu_M^\ell + \sum_{k=2}^{N_E} J_k(t)\mathbf{C}_k^M + \sum_{m=1}^{N_T} J_m^T(t)\mathbf{T}_m^M\,, \tag{37}$$

where

- $\mathbf{H}_0(t) \in \boldsymbol{H}_{\Gamma\setminus\Gamma_E}(\mathbf{curl}, \Omega) := \{\mathbf{V} \in \boldsymbol{H}(\mathbf{curl}, \Omega) : \boldsymbol{\gamma}_\times\mathbf{V} = 0 \text{ on } \Gamma \setminus \Gamma_E\}$ is the magnetic field in the interior of Ω and at the electric ports,
- $\rho_M(t) \in \widetilde{H}^{1/2}_{\Gamma_M}(\Gamma_I) := \{\psi \in H^{\frac{1}{2}}(\Gamma_I \cup \Gamma_M) : \psi = 0 \text{ on } \Gamma_M\}$ is a magnetic scalar surface potential on Γ_I,
- $\nu_M^\ell \in H^{\frac{1}{2}}(\partial\Omega)$ is equal to 1 on Γ_M^ℓ, and zero on all other magnetic parts and all electric ports.
- $\mathbf{C}_k^M \in \boldsymbol{H}(\mathbf{curl}, \Omega)$ extends the surface co-homology vectorfield $\mathbf{c}_k^M$: $\boldsymbol{\gamma}_\times\mathbf{C}_k^M = \mathbf{c}_k^M$, $k = 2, \dots, N_E$.
- $\mathbf{T}_m^M$ is an $\boldsymbol{H}(\mathbf{curl}, \Omega)$-extension of $\mathbf{t}_m^H$: $\boldsymbol{\gamma}_\times\mathbf{T}_m^M = \mathbf{t}_m^M$.

The expressions (32d) and (32a) pave the way for the following replacements of the three path integrals in (28), analogous to (35):

$$\int_{\partial\Gamma_M^\ell} \mathbf{E} \cdot \mathrm{d}\boldsymbol{s} \;\longrightarrow\; \dot{B}_\ell\,, \quad \int_{\gamma_k^M} \boldsymbol{\gamma_t}\mathbf{E} \cdot \mathrm{d}\boldsymbol{s} \;\longrightarrow\; U_k\,, \quad \int_{\hat{\tau}_m} \boldsymbol{\gamma_t}\mathbf{E} \cdot \mathrm{d}\boldsymbol{s} \;\longrightarrow\; \dot{B}_m^T\,. \tag{38}$$

As before, the smoothness requirements for $\mathbf{E}$ and $\mathbf{E}'$ in (28) are relaxed and we merely demand $\mathbf{E}, \mathbf{E}' \in \boldsymbol{L}^2(\Omega)$. This leads to the final $\mathbf{H}$-based variational formulation taking into account port quantitites:

Seek $\mathbf{H}_0 : [0,T] \to \boldsymbol{H}_{\Gamma\setminus\Gamma_E}(\mathbf{curl},\Omega)$, $\rho_M : [0,T] \to \widetilde{H}^{1/2}_{\Gamma_M}(\Gamma_I)$, $F_\ell : [0,T] \to \mathbb{R}$, $J_k : [0,T] \to \mathbb{R}$, $J_m^T : [0,T] \to \mathbb{R}$, $\mathbf{H} : [0,T] \to \boldsymbol{L}^2(\Omega)$

$$\int_\Omega \partial_t(\mu\mathbf{H})(t) \cdot \mathbf{H}_0' + \mathbf{E}(t) \cdot \mathbf{curl}\,\mathbf{H}_0' \,\mathrm{d}\boldsymbol{x} = 0\,, \tag{39a}$$

$$\int_\Omega \partial_t(\mu\mathbf{H})(t) \cdot \mathbf{grad}\,\mathsf{X}\rho_M' \,\mathrm{d}\boldsymbol{x} = 0\,, \tag{39b}$$

$$\int_\Omega \partial_t(\mu\mathbf{H})(t) \cdot \mathbf{grad}\,\mathsf{X}\nu_M^\ell \,\mathrm{d}\boldsymbol{x} \quad -\dot{B}_\ell(t) = 0\,, \tag{39c}$$

$$\int_\Omega \partial_t(\mu\mathbf{H})(t) \cdot \mathbf{C}_M^k + \mathbf{E} \cdot \mathbf{curl}\,\mathbf{C}_M^k \,\mathrm{d}\boldsymbol{x} \quad -U_k(t) = 0\,, \tag{39d}$$

$$\int_\Omega \partial_t(\mu\mathbf{H})(t) \cdot \mathbf{T}_M^m + \mathbf{E}(t) \cdot \mathbf{curl}\,\mathbf{T}_M^m \,\mathrm{d}\boldsymbol{x} \quad -\dot{B}_m^T(t) = 0\,, \tag{39e}$$

$$\int_\Omega \big(\partial_t(\epsilon\mathbf{E})(t) + \sigma\mathbf{E}(t)\big) \cdot \mathbf{E}' - \mathbf{curl}\,\mathbf{H}(t) \cdot \mathbf{E}' \,\mathrm{d}\boldsymbol{x} = 0 \tag{39f}$$

for all $\mathbf{H}_0' \in \boldsymbol{H}(\mathrm{curl}_\Gamma,\Gamma)\Gamma\setminus\Gamma_E$, $\rho_M' \in \widetilde{H}^{1/2}_{\Gamma_M}(\Gamma_I)$, $\ell = 1,\ldots,N_M$, $k = 2,\ldots,N_E$, $m = 1,\ldots,N_T$, $\mathbf{E}' \in \boldsymbol{L}^2(\Omega)$, and $\mathbf{H} = \mathbf{H}(\mathbf{H}_0,\rho_M,F_\ell,J_k,J_m^T)$ as in (37).

Also here we face "six equations versus nine unknowns" and either fixing port quantities, aka, imposing excitation through sources, or adding circuit equations will remedy this imbalance. I goes without saying that here we can eliminate the electric field $\mathbf{E}$, *cf.* Remark 7.

5.3 | Power Balance

Conservation of energy is a guiding principle in the coupling of fields and circuits [5, 4]. It is also respected in the variational formulations (36) and (39). We elaborate this for the $\mathbf{E}$-based formulation (36).

The idea is to set $\mathbf{E}' := \mathbf{E}(t)$ and $\mathbf{H}' := \mathbf{H}(t)$ in (24) and add both resulting equations taking into account (32) and (34)

$$J_k(t) = \int_{\partial\Gamma_E^k} \mathbf{H}(t) \cdot \mathrm{d}s\,, \quad F_\ell(t) = \int_{\widehat{\gamma}_\ell^E} \mathbf{H}(t) \cdot \mathrm{d}s\,, \quad J_m^T(t) = \int_{\widehat{\tau}_m} \mathbf{H}(t) \cdot \mathrm{d}s\,.$$

This gives us the power balance relation

$$\begin{aligned}\frac{d}{dt}\int_\Omega \tfrac{1}{2}\epsilon\mathbf{E}(t)\cdot\mathbf{E}(t) + \tfrac{1}{2}\mu\mathbf{H}(t)\cdot\mathbf{H}(t)\,\mathrm{d}\boldsymbol{x} + \int_\Omega \sigma\mathbf{E}(t)\cdot\mathbf{E}(t)\,\mathrm{d}\boldsymbol{x}\\ = \int_\Omega \partial_t(\epsilon\mathbf{E})(t)\cdot\mathbf{E}(t) + \partial_t(\mu\mathbf{H})(t)\cdot\mathbf{H}(t) + \sigma\mathbf{E}(t)\cdot\mathbf{E}(t)\,\mathrm{d}\boldsymbol{x}\\ = \sum_{k=1}^{N_E} U_k(t)J_k(t) + \sum_{\ell=1}^{\beta_M} \dot{B}_\ell(t)F_\ell(t) + \sum_{m=1}^{N_T} J_m^T(t)\dot{B}_m^T(t)\,.\end{aligned} \tag{40}$$

The products of port quantities give the power flux through each port, which is offset by a change in the electromagnetic field energies and Ohmic losses. We observe that the six types of port quantities can be arranged into three pairs, products of whose components yield power fluxes. The same arguments can be employed for the $\mathbf{H}$-based model.

Remark 8. In the case $\Gamma_R \neq \emptyset$ another term of the form

$$\int_{\Gamma_R} \big(\mathsf{Z}^{-1}(\boldsymbol{\gamma_t}\mathbf{E})\big)(t) \cdot \boldsymbol{\gamma_t}\mathbf{E}(t)\,\mathrm{d}S = \int_{\Gamma_R} \big(\mathsf{Z}(\boldsymbol{\gamma}_\times\mathbf{H})\big)(t) \cdot \boldsymbol{\gamma}_\times\mathbf{H}(t)\,\mathrm{d}S \tag{41}$$

emerges on the right-hand side of (40). Straightforwardly, it arises from (29). It represents the power carried off by electromagnetic radiation.

6 | FINITE-ELEMENT GALERKIN DISCRETIZATION: LOWEST-ORDER SCHEME

The variational problems (36) and (39) immediately lend themselves to a Galerkin discretization by means of conforming finite elements on a tetrahedral mesh $\mathcal{M}$ of Ω, which *resolves the ports* in the sense that every Γ_E^k and Γ_M^ℓ is the union of faces of mesh cells. All geometric entities of the mesh are to be endowed with an intrinsic orientation.

We restrict the discussion to the $\mathbf{E}$-based model (36) and leave the analogous considerations for the $\mathbf{H}$-based model (39) to the reader. We also focus on lowest-order finite-element approximation, known as edge elements/Whitney-1-forms in the case of finite-element subspaces of $\boldsymbol{H}(\mathbf{curl},\Omega)$ [25, Sect. 3]. Their locally supported basis functions, dubbed "edge basis functions" in the sequel, are associated with edges of $\mathcal{M}$. We

remind that edge elements admit discrete potentials and the relevant discrete scalar potentials are provided by $\mathcal{M}$-piecewise linear continuous functions. Those can be written as linear combinations of node-associated locally supported basis functions. We refer to them as "tent functions".

The following finite-dimensional trial and test space can be used in (36):

- $\boldsymbol{H}_{\Gamma\setminus\Gamma_M}(\mathbf{curl},\Omega)$ is replaced with the space $\mathcal{E}_h$ spanned by edge basis functions associated with Ω-interior edges of $\mathcal{M}$ plus edges in the interior of magnetic ports.
- The finite element subspace of $\widetilde{H}^{1/2}_{\Gamma_E}(\Gamma_I)$ is generated by the traces of those tent functions belonging to the nodes located in the interior of Γ_I and on $\partial\Gamma_M$. We write $\mathcal{S}_h$ for their span.
- For the finite-element approximation of $\boldsymbol{L}^2(\Omega)$ we simply use the space $\mathcal{C}_h$ of $\mathcal{M}$-piecewise constant vectorfields.

The equations (36b) and (36c) feature the extension operator X. In the finite-element setting we use simple nodal truncation: extension of a $\mathcal{M}|_\Gamma$-piecewise linear function is done by keeping all nodal values on Γ and setting the contributions of all tent functions at nodes in the interior of Ω to zero.

The next isssue is the representation of the special functions ν^k_E and $\mathbf{C}^M_\ell$ occurring in (36c) and (36d), respectively. Those are defined in the paragraph following (34). The function ν^k_E is simply given as the sum of all tent functions belonging to mesh nodes contained in $\overline{\Gamma}^k_E$. Note the closure of the set! The partition-of-unity property of the tent function yields the desired properties of the resulting $\mathcal{M}$-piecewise linear function $\mathsf{X}\nu^k_E$.

The construction of $\mathbf{C}^E_\ell$ and $\mathbf{T}^E_m$ is more challenging. It follows recipes already developed in [21]: As explained in Section 3.4 to every $\mathbf{C}^E_\ell$ there is an associated dual cycle γ^M_ℓ of class (CM), which is an oriented curve. The same applies to every $\mathbf{T}^E_m$ and its dual cycle is also of class (T).

Assumption 4. We assume that every cycle γ^M_ℓ, $\ell = 2,\ldots,N_M$, γ^E_k, $k = 2,\ldots,N_E$, and τ_m, $m = 1,\ldots,N_T$, is a chain of edges of $\mathcal{M}$.

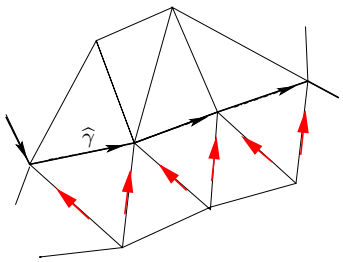

FIGURE 7 Close-up of the collar field $\mathbf{c}^E$ skirting the dual cycle $\widehat{\gamma}$. The red arrows indicate the edges whose edge basis functions will contribute to $\mathbf{c}^E$ with weight $+1$.

This assumption can always be met, provided that the mesh resolves the topology of Ω. Given a dual cycle $\widehat{\gamma}/\widehat{\tau}_m$ as an edge chain $\subset\ \Gamma$, we can choose the associated co-homology vector fields $\mathbf{c}^E_\ell/\mathbf{t}^E_m$ as so-called collar fields supported in the triangles adjacent to the dual cycle $\widehat{\gamma}$ on "the right side". For details refer to Figure 7 and [21]. Afterwards we employ simple nodal truncation to extend them to finite-element vectorfields on Ω.

Then, given the collar fields $\mathbf{c}^E_\ell$, we obtain $\mathbf{C}^E_\ell$ by simply retaining the weights of the edge basis functions on Γ and setting all those for interior edge basis functions to zero, which is the "trivial finite-element extension procedure". The same construction applies to $\mathbf{T}^E_m$.

Remark 9. Note that collar fields are extremely sparse under the reasonable assumption that the edge cycles do not behave like surface-filling curves: viewed as finite-element functions only a few degrees of freedom will be non-zero in the edge basis representations of the collar fields.

Finally, let us exhibit the structure of the semi-discrete evolution problem for the $\mathbf{E}$-based formulation, an ordinary differential equation for the basis expansion coefficients of the unknown fields plus the port quantities. To that end we introduce the time-dependent coefficient vectors

- $\vec{E} = \vec{E}(t) \in \mathbb{R}^{n_E}$ for the time-dependent vector of edge-basis expansion coefficients of $\mathbf{E}_{0,h} : [0,T] \to \mathcal{E}_h$, $n_E := \dim \mathcal{E}_h$,
- $\vec{\rho} = \vec{\rho}(t) \in \mathbb{R}^{n_S}$ for the tent-basis expansion coefficient vector of $\mathsf{X}\rho_{E,h} : [0,T] \to \mathcal{S}_h$, $n_S := \dim \mathcal{S}_h$,
- $\vec{H} = \vec{H}(t) \in \mathbb{R}^{n_H}$ for the vector of cell values of $\mathbf{H}_h : [0,T] \to \mathcal{C}_h$, $n_H := \dim \mathcal{C}_h$,
- $\vec{U}(t) := (U_2(t),\ldots,U_{N_E}(t))^\top \in \mathbb{R}^{N_E-1}$ (electric port potentials),
  $\vec{B}(t) = (\dot{B}_1(t),\ldots,\dot{B}_{N_M-1}(t))^\top \in \mathbb{R}^{N_M-1}$ (magnetic port fluxes),
  $\vec{L}(t) = (\dot{B}^T_1(t),\ldots,\dot{B}^T_{N_T}(t)) \in \mathbb{R}^{N_T}$ (linked magnetic fluxes),
- $\vec{J}(t) = (J_2(t),\ldots,J_{N_E}(t))^\top \in \mathbb{R}^{N_E-1}$ (electric port currents),
  $\vec{F}(t) = (F_2(t),\ldots,F_{N_M}(t))^\top \in \mathbb{R}^{N_M-1}$ (port M.M.F.s),
  $\vec{I}(t) = (J^T_1(t),\ldots,J^T_{N_T}(t))^\top \in \mathbb{R}^{N_T}$ (linked electric currents).

$$\begin{pmatrix} \mathbf{M}_{EE} & \mathbf{M}_{\rho E} & \mathbf{M}_{UE} & \mathbf{M}_{BE} & \mathbf{M}_{LE} & \mathbf{O} \\ \mathbf{M}_{\rho E}^\top & \mathbf{M}_{\rho\rho} & \mathbf{M}_{U\rho} & \mathbf{M}_{B\rho} & \mathbf{M}_{L\rho} & \mathbf{O} \\ \mathbf{M}_{UE}^\top & \mathbf{M}_{U\rho}^\top & \mathbf{M}_{UU} & \mathbf{M}_{BU} & \mathbf{M}_{LU} & \mathbf{O} \\ \mathbf{M}_{BE}^\top & \mathbf{M}_{B\rho}^\top & \mathbf{M}_{BU}^\top & \mathbf{M}_{BB} & \mathbf{M}_{LB} & \mathbf{O} \\ \mathbf{M}_{LE}^\top & \mathbf{M}_{L\rho}^\top & \mathbf{M}_{LU}^\top & \mathbf{M}_{LB}^\top & \mathbf{M}_{LL} & \mathbf{O} \\ \mathbf{O} & \mathbf{O} & \mathbf{O} & \mathbf{O} & \mathbf{O} & \mathbf{M}_{HH} \end{pmatrix} \frac{d}{dt} \begin{pmatrix} \vec{E} \\ \vec{\rho} \\ \vec{U} \\ \vec{B} \\ \vec{L} \\ \vec{H} \end{pmatrix} + \begin{pmatrix} \mathbf{R}_{EE} & \mathbf{R}_{\rho E} & \mathbf{R}_{UE} & \mathbf{R}_{BE} & \mathbf{R}_{LE} & -\mathbf{C} \\ \mathbf{R}_{\rho E}^\top & \mathbf{R}_{\rho\rho} & \mathbf{R}_{U\rho} & \mathbf{R}_{B\rho} & \mathbf{R}_{L\rho} & \mathbf{O} \\ \mathbf{R}_{UE}^\top & \mathbf{R}_{U\rho}^\top & \mathbf{R}_{UU} & \mathbf{R}_{BU} & \mathbf{R}_{LU} & \mathbf{O} \\ \mathbf{R}_{BE}^\top & \mathbf{R}_{B\rho}^\top & \mathbf{R}_{BU}^\top & \mathbf{R}_{BB} & \mathbf{R}_{LB} & -\mathbf{Q} \\ \mathbf{R}_{LE}^\top & \mathbf{R}_{L\rho}^\top & \mathbf{R}_{LU}^\top & \mathbf{R}_{LB}^\top & \mathbf{R}_{LL} & -\mathbf{P} \\ \mathbf{C}^\top & \mathbf{O} & \mathbf{O} & \mathbf{Q}^\top & \mathbf{P}^\top & \mathbf{O} \end{pmatrix} \begin{pmatrix} \vec{E} \\ \vec{\rho} \\ \vec{U} \\ \vec{B} \\ \vec{L} \\ \vec{H} \end{pmatrix} = \begin{pmatrix} 0 \\ 0 \\ \vec{J} \\ \vec{F} \\ \vec{I} \\ 0 \end{pmatrix} . \tag{42}$$

The mass matrices $\mathbf{M}_{**}$, $*,\star \in \{E,\rho,U,B,L\}$ arise from the Galerkin discretization of the bilinear form $(\mathbf{E},\mathbf{E}') \mapsto \int_\Omega \epsilon(\boldsymbol{x})\mathbf{E}\cdot\mathbf{E}'\,\mathrm{d}\boldsymbol{x}$, with the exception of $\mathbf{M}_{HH} \in \mathbb{R}^{n_H,n_H}$, which is a discretization of $(\mathbf{H},\mathbf{H}') \mapsto \int_\Omega \mu(\boldsymbol{x})\mathbf{H}\cdot\mathbf{H}'\,\mathrm{d}\boldsymbol{x}$ on $\mathcal{C}_h \times \mathcal{C}_h$. The matrices $\mathbf{R}_{**}$, $*,\star \in \{E,\rho,U,B,L\}$ are produced by the Galerkin discretization of the Ohmic loss blinear form $(\mathbf{E},\mathbf{E}') \mapsto \int_\Omega \sigma(\boldsymbol{x})\mathbf{E}\cdot\mathbf{E}'\,\mathrm{d}\boldsymbol{x}$ on the spaces indicated by the subscripts.

The matrices $\mathbf{C} \in \mathbb{R}^{n_E,n_H}$ represent a discrete $\mathbf{curl}$-operator obtained by the Galerkin discretization of $(\mathbf{H},\mathbf{E}') \mapsto \int_\Omega \mathbf{H}\cdot\mathbf{curl}\,\mathbf{E}'\,\mathrm{d}\boldsymbol{x}$ on $\mathcal{C}_h \times \mathcal{E}_h$. The entries of the matrix $\mathbf{Q} \in \mathbb{R}^{N_M-1,n_H}$ arise from plugging the basis functions of $\mathcal{C}_h$ into the linear forms $\mathbf{H} \mapsto \int_\Omega \mathbf{H}\cdot\mathbf{curl}\,\mathbf{C}_\ell^E\,\mathrm{d}\boldsymbol{x}$, $\ell = 2,\ldots,N_M$, and we get $\mathbf{P} \in \mathbb{R}^{N_T,n_H}$ from the Galerkin discretization of $(\mathbf{H},\mathbf{E}') \mapsto \int_\Omega \mathbf{H}\cdot\mathbf{curl}\,\mathbf{E}'\,\mathrm{d}\boldsymbol{x}$ on $\mathcal{C}_h \times \mathrm{span}\{\mathbf{T}_1^E,\ldots,\mathbf{T}_{N_T}^E\}$.

Remark 10. We consider the semi-discrete $\mathbf{E}$-based model (42) in frequency domain at a fixed frequency $f = \frac{\omega}{2\pi}, \omega > 0$. This amounts to replacing $\partial_t \to \cdot i\omega$ and treating all quantities as complex amplitudes (phasors). Thus the ordinary differential equation (42) is converted into the linear system

$$\left(\begin{array}{ccc|ccc} i\omega\mathbf{M}_{EE}+\mathbf{R}_{EE} & i\omega\mathbf{M}_{\rho E}+\mathbf{R}_{\rho E} & -\mathbf{C} & i\omega\mathbf{M}_{UE}+\mathbf{R}_{UE} & i\omega\mathbf{M}_{BE}+\mathbf{R}_{BE} & i\omega\mathbf{M}_{LE}+\mathbf{R}_{LE} \\ i\omega\mathbf{M}_{\rho E}^\top+\mathbf{R}_{\rho E}^\top & i\omega\mathbf{M}_{\rho\rho}+\mathbf{R}_{\rho\rho} & \mathbf{O} & i\omega\mathbf{M}_{U\rho}+\mathbf{R}_{U\rho} & i\omega\mathbf{M}_{B\rho}+\mathbf{R}_{B\rho} & i\omega\mathbf{M}_{L\rho}+\mathbf{R}_{L\rho} \\ \mathbf{C}^\top & \mathbf{O} & i\omega\mathbf{M}_{HH} & \mathbf{O} & \mathbf{Q}^\top & \mathbf{P}^\top \\ \hline i\omega\mathbf{M}_{UE}^\top+\mathbf{R}_{UE}^\top & i\omega\mathbf{M}_{U\rho}^\top+\mathbf{R}_{U\rho}^\top & \mathbf{O} & i\omega\mathbf{M}_{UU}+\mathbf{R}_{UU} & i\omega\mathbf{M}_{BU}+\mathbf{R}_{BU} & i\omega\mathbf{M}_{LU}+\mathbf{R}_{LU} \\ i\omega\mathbf{M}_{BE}^\top+\mathbf{R}_{BE}^\top & i\omega\mathbf{M}_{B\rho}^\top+\mathbf{R}_{B\rho}^\top & -\mathbf{Q} & i\omega\mathbf{M}_{BU}^\top+\mathbf{R}_{BU}^\top & i\omega\mathbf{M}_{BB}+\mathbf{R}_{BB} & i\omega\mathbf{M}_{LB}+\mathbf{R}_{LB} \\ i\omega\mathbf{M}_{LE}^\top+\mathbf{R}_{LE}^\top & i\omega\mathbf{M}_{L\rho}^\top+\mathbf{R}_{L\rho}^\top & -\mathbf{P} & i\omega\mathbf{M}_{LU}^\top+\mathbf{R}_{LU}^\top & i\omega\mathbf{M}_{LB}^\top+\mathbf{R}_{LB}^\top & i\omega\mathbf{M}_{LL}+\mathbf{R}_{LL} \end{array}\right) \begin{pmatrix} \vec{E} \\ \vec{\rho} \\ \vec{H} \\ \vec{U} \\ \vec{B} \\ \vec{L} \end{pmatrix} = \begin{pmatrix} 0 \\ 0 \\ 0 \\ \vec{J} \\ \vec{F} \\ \vec{I} \end{pmatrix} . \tag{43}$$

Provided that the left-upper block indicated in (43) is invertible, which may not be the case for particular "resonant" wavenumbers ω, we can eliminate the unknowns $\vec{E}$, $\vec{\rho}$, and $\vec{H}$ by *static condensation* and obtain a Schur-complement linear system. Condensing the matrix blocks on (43) into $\mathbb{A}$, $\mathbb{B}$, $\mathbb{C}^\top$, and $\mathbb{D}$, and writing $\mathfrak{X} := \left(\vec{E},\vec{\rho},\vec{H}\right)$, $\mathfrak{P} := \left(\vec{U},\vec{B},\vec{L}\right)$, $\mathfrak{Q} := \left(\vec{J},\vec{F},\vec{I}\right)$, this procedure can be cast into the following formulas:

$$(43) \quad \Leftrightarrow \quad \left(\begin{array}{c|c} \mathbb{A} & \mathbb{B} \\ \hline \mathbb{C}^\top & \mathbb{D} \end{array}\right) \begin{pmatrix} \vec{\mathfrak{X}} \\ \vec{\mathfrak{P}} \end{pmatrix} = \begin{pmatrix} 0 \\ \vec{\mathfrak{Q}} \end{pmatrix} \quad \Rightarrow \quad \boxed{\left(\mathbb{D} - \mathbb{C}^\top \mathbb{A}^{-1} \mathbb{B}\right)} \vec{\mathfrak{P}} = \mathfrak{Q} \, . \tag{44}$$

The highlighted Schur-complement $(N_E + N_M + N_T - 2) \times (N_E + N_M + N_T - 2)$ matrix is a lumped-element multi-port model of the field domain and its entries can be viewed as generalized impedances, capacities, inductances, etc.

Remark 11. An analysis of the accuracy of solutions of the semi-discrete problem (42) is outside the scope of this work. Please refer to works on the numerical analysis of finite-element methods for Maxwell's equations, for example [16]. For the finite-element scheme presented above we expect first order convergence in the meshwidth, if the field solutions are sufficiently smooth.

7 | NUMERICAL TEST: E-BASED FORMULATION

We discuss a conrete simulation in *frequency domain* at fixed frequencies $f = \frac{\omega}{2\pi} = 50, 200, 1000\mathrm{Hz}$. We rely on the $\mathbf{E}$-based model (36) and replace $\partial_t \to \cdot i\omega$ and regard all fields and port quantities as complex-valued phasors. We consider the particular geometry displayed in Figure 8, which means $N_E = 2$, $N_M = 0$, and $N_T = 2$. Topologically, this resembles the situation of Figure 6.

We short-circuit the electric ports, which amounts to imposing $U_2 = 0$ in the notations of Section 5.1 and in all simulations drive the system by through a linked magnetic flux $\dot{B}_1^T = (3.518 \cdot 10^{-3} + 1.893 \cdot 10^{-4} i)\mathrm{V}$ (RMS $0.03518\mathrm{V}$) penetrating the surface bounded by τ_1. This is equivalent to imposing an electromotive force along τ_1, see (32e). Such excitation can model the effect of a current-carrying coil outside the field domain.

We end up with a special frequency-domain version of (36). Given $\dot{B}_1^T \in \mathbb{C}$ seek[5]

$$\mathbf{E} = \mathbf{E}_0 + \mathbf{grad}\,\mathsf{X}\rho_E + \dot{B}_1^T \mathbf{T}_1^E + \dot{B}_2^T \mathbf{T}_2^E \quad [\, + U_2\,\mathbf{grad}\,\mathsf{X}\nu_E^2\,] \tag{45}$$

[5] Unknowns are marked with purple color.

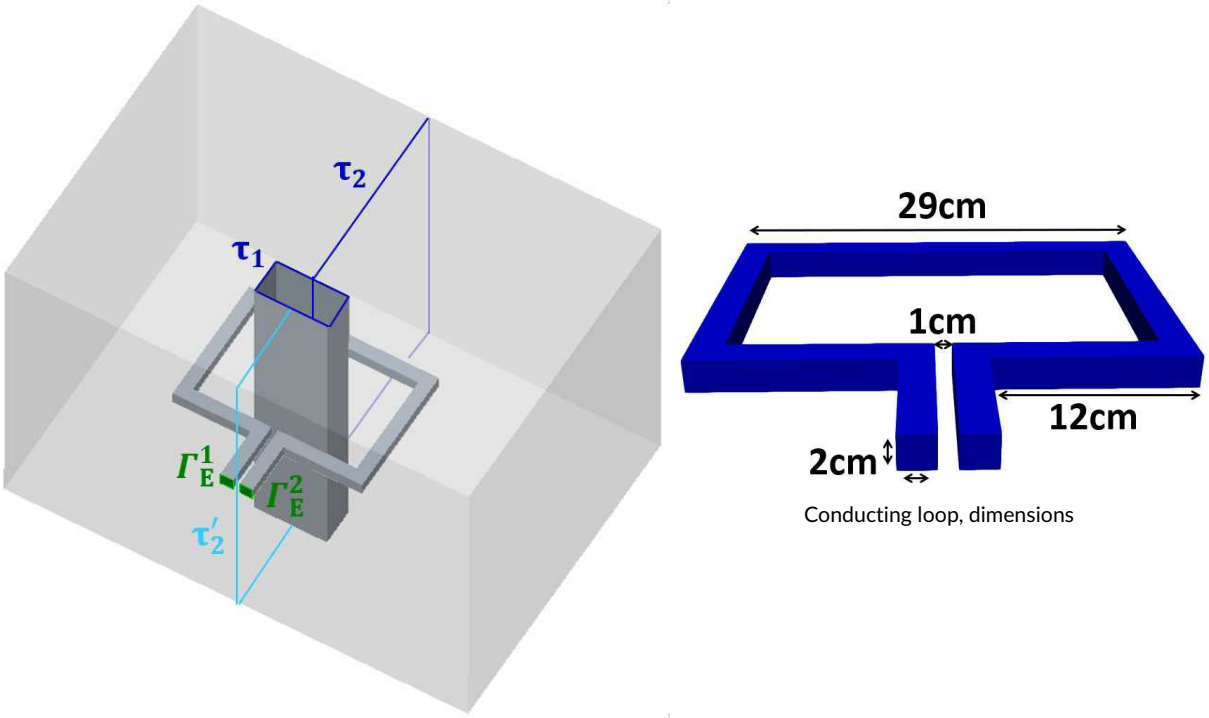

FIGURE 8 Geometry for numerical demonstration: bounded field domain Ω with the shape of a "cubistic torus" ($N_T = 2$), whose complement represents the unbounded circuit domain Ω_C. Central tunnel surrounded by conducting split loop, connected to two electric ports ($N_E = 2$). Conductivity $\sigma = 10^6\,\mathrm{A/Vm}$ inside loop, $\sigma = 0$ outside, $\mu = \mu_0$, $\epsilon = \epsilon_0$ everywhere, which leads to an approximate resistance of $R = 2.48\mathrm{m}\Omega$ and inductance of $L = 0.45\mu\mathrm{H}$. The topological cycles τ_1, τ_2 are marked in blue, an alternative topological cycle τ_2' in cyan. Note that τ_2' runs through the small gap between the electric ports.

with $\mathbf{E}_0 \in \boldsymbol{H}_0(\mathbf{curl}, \Omega)$, $\rho_E \in \widetilde{H}^{1/2}_{\Gamma_E}(\Gamma_I)$, $\dot{B}_2^T \in \mathbb{C}$, and $\mathbf{H} \in \boldsymbol{L}^2(\Omega)$, $J_2^T \in \mathbb{C}$ such that

$$\int_\Omega \big(i\omega\epsilon(\boldsymbol{x}) + \sigma(\boldsymbol{x})\big)\mathbf{E}\cdot\mathbf{E}_0' - \mathbf{H}\cdot\mathbf{curl}\,\mathbf{E}_0'\,\mathrm{d}\boldsymbol{x} = 0\,, \tag{46a}$$

$$\int_\Omega \big(i\omega\epsilon(\boldsymbol{x}) + \sigma(\boldsymbol{x})\big)\mathbf{E}\cdot\mathbf{grad}\,\mathsf{X}\rho_E'\,\mathrm{d}\boldsymbol{x} = 0\,, \tag{46b}$$

$$\int_\Omega \big(i\omega\epsilon(\boldsymbol{x}) + \sigma(\boldsymbol{x})\big)\mathbf{E}\cdot\mathbf{T}_2^E - \mathbf{H}\cdot\mathbf{curl}\,\mathbf{T}_2^E\,\mathrm{d}\boldsymbol{x} - J_2^T = 0\,, \tag{46c}$$

$$\int_\Omega \big(i\omega\mu(\boldsymbol{x})\mathbf{H} + \mathbf{curl}\,\mathbf{E}\big)\cdot\mathbf{H}'\,\mathrm{d}\boldsymbol{x} = 0 \tag{46d}$$

for all $\mathbf{E}_0' \in \boldsymbol{H}_0(\mathbf{curl}, \Omega)$, $\rho_E' \in \widetilde{H}^{1/2}_{\Gamma_E}(\Gamma_I)$, and $\mathbf{H}' \in \boldsymbol{L}^2(\Omega)$. In (45) we have hinted that the voltage drop between the electric ports is imposed, though in this example $U_2 = 0$. This removes a degree of freedom from the trial space for $\mathbf{E}$, which forces us to remove the corresponding one from the test space. As a consequence (36c) does not contribute to the variational equations.

Next, we eliminate the magnetic field $\mathbf{H}$ as discussed in Remark 7 by testing (46d) with $\mathbf{H}' := \mathbf{curl}\,\mathbf{E}_0'$ and $\mathbf{H}' := \mathbf{curl}\,\mathbf{T}_2^E$, respectively, and, similar to [8, Sect. 3], obtain: Seek $\mathbf{E}$ as defined in (45) and $J_2^T \in \mathbb{C}$ such that

$$\int_\Omega \big(i\omega\epsilon(\boldsymbol{x}) + \sigma(\boldsymbol{x})\big)\mathbf{E}\cdot\mathbf{E}_0' + \frac{1}{i\omega\mu(\boldsymbol{x})}\,\mathbf{curl}\,\mathbf{E}\cdot\mathbf{curl}\,\mathbf{E}_0'\,\mathrm{d}\boldsymbol{x} = 0\,, \tag{47a}$$

$$\int_\Omega \big(i\omega\epsilon(\boldsymbol{x}) + \sigma(\boldsymbol{x})\big)\mathbf{E}\cdot\mathbf{grad}\,\mathsf{X}\rho_E'\,\mathrm{d}\boldsymbol{x} = 0\,, \tag{47b}$$

$$\int_\Omega \big(i\omega\epsilon(\boldsymbol{x}) + \sigma(\boldsymbol{x})\big)\mathbf{E}\cdot\mathbf{T}_2^E + \frac{1}{i\omega\mu(\boldsymbol{x})}\,\mathbf{curl}\,\mathbf{E}\cdot\mathbf{curl}\,\mathbf{T}_2^E\,\mathrm{d}\boldsymbol{x} - J_2^T = 0 \tag{47c}$$

for all $\mathbf{E}_0' \in \boldsymbol{H}_0(\mathbf{curl}, \Omega)$ and $\rho_E' \in \widetilde{H}^{1/2}_{\Gamma_E}(\Gamma_I)$.

The unknown J_2^T represents the complex amplitude of the total current flowing through τ_2, whereas $\dot{B}_2^T$ from (45) is the electromotive force around τ_2. The complex amplitude of the current J_2 flowing through the electric ports can be recovered from (36c):

$$J_2 = \int_\Omega (i\omega\epsilon(\boldsymbol{x}) + \sigma(\boldsymbol{x}))\,\mathbf{E}\cdot\mathbf{grad}\,\mathsf{X}\nu_E^2\,\mathrm{d}\boldsymbol{x}\;, \tag{48}$$

where ν_E^2 has been specified in Section 5.1.

The finite-element Galerkin discretization of (47) is carried out precisely as described in Section 6 using three tetrahedral meshes of increasing resolution. The mutually dual topological cycles τ_1 and τ_2 directly enter the model through the co-homology vector fields $\mathbf{T}_1^E$ and $\mathbf{T}_2^E$, which we constructed as "collar fields" skirting the dual cycle according to the algorithm outlined in Figure 7. We choose both τ_1 and τ_2 as flat rectangles as indicated in Figure 8. For the cycle τ_2 we explore two options,

(i) the cycle bounds a flat surface cutting the conductor, τ_2 in Figure 8,

(ii) the cycle runs between the contacts and the associated surface cuts through the air gap of the split conducting loop, τ_2' in Figure 8.

7.1 | Validation: Comparison with Circuit Model

In good approximation the conducting loop can modeled as a linear circuit element with resistance $R = 2.488\cdot 10^{-3}\Omega$, inductance $L = 4.261\cdot 10^{-7}\mathrm{H}$, and vanishing capacitance. These values were determined at $\omega = 1\mathrm{Hz}$ by means of a high-resolution finite-element computation[6]. Thus, we can obtain the resulting frequency-dependent loop current as $I = U/Z$ with U standing for the voltage drop along the loop and Z for the impedance $R + i\omega L$. In our new method we impose the voltage drop through $\dot{B}_1^T$ and recover the loop current as the unknown J_2^T. Table 1 shows the results for the exciting voltage amplitude $U = \dot{B}_1^T = (3.518\cdot 10^{-3} + 1.893\cdot 10^{-4}i)\mathrm{V}$. The results of all computations are in excellent agreement with the predictions of the circuit model for three different frequencies.

	No. of tets.	loop current for $\omega = 50\mathrm{Hz}$	loop current for $\omega = 200\mathrm{Hz}$	loop current for $\omega = 1000\mathrm{Hz}$
coarse mesh	298777	$(-1.419 - 2.720i\cdot 10^{-4})\mathrm{A}$	$(-1.372 + 0.218i)\mathrm{A}$	$(-0.699 + 0.666i)\mathrm{A}$
medium mesh	347391	$(-1.418 - 7.781\cdot 10^{-5}i)\mathrm{A}$	$(-1.370 + 0.218i)\mathrm{A}$	$(-0.696 + 0.666i)\mathrm{A}$
fine mesh	599105	$(-1.414 - 1.001\cdot 10^{-7})\mathrm{A}$	$(-1.367 + 0.2180i)\mathrm{A}$	$(-0.699 + 0.665i)\mathrm{A}$
circuit model, $I = U/Z$		$(-1.414 - 3.265\cdot 10^{-6})\mathrm{A}$	$(-1.367 + 0.218i)\mathrm{A}$	$(-0.694 + 0.670i)\mathrm{A}$

TABLE 1 Complex amplitudes of currents flowing in the square loop conductor at different frequencies; the results in the top three rows were obtained by our new method and finite-element Galerkin discretization as described in the main text.

7.2 | Case study: Excitation by Linked Fluxes

We study the impact of the choice of cycles. For both options (i) and (ii) we visualize the electric currents in Figure 9 and tabulate J_2^T for different meshes in Table 2.

		50Hz		200Hz		1000Hz	
	No. of tets	J_2 for τ_2	J_2 for τ_2'	J_2 for τ_2	J_2 for τ_2'	J_2 for τ_2	J_2 for τ_2'
coarse mesh	298777	1.0034	$1.2\cdot 10^{-10}$	0.9822	$3.1\cdot 10^{-8}$	0.6827	$5.3\cdot 10^{-10}$
medium mesh	347391	1.0023	$1.1\cdot 10^{-10}$	0.9810	$3.0\cdot 10^{-8}$	0.6811	$5.7\cdot 10^{-10}$
fine mesh	599105	0.9999	$5.4\cdot 10^{-9}$	0.9787	$5.1\cdot 10^{-8}$	0.6793	$1..1\cdot 10^{-9}$

TABLE 2 RMS currents J_2^T for different choices of the topological cycles bounding w.r.t. Ω, see Figure 8, and computed on tetrahedral meshes with different resolutions. The large fluctuations of the minute values of J_2^T are due to discretization errors. Same currents as in Table 1 when choosing cycle τ_2.

[6]The computations relied on the code Hadapt developedf at ABB Corp.

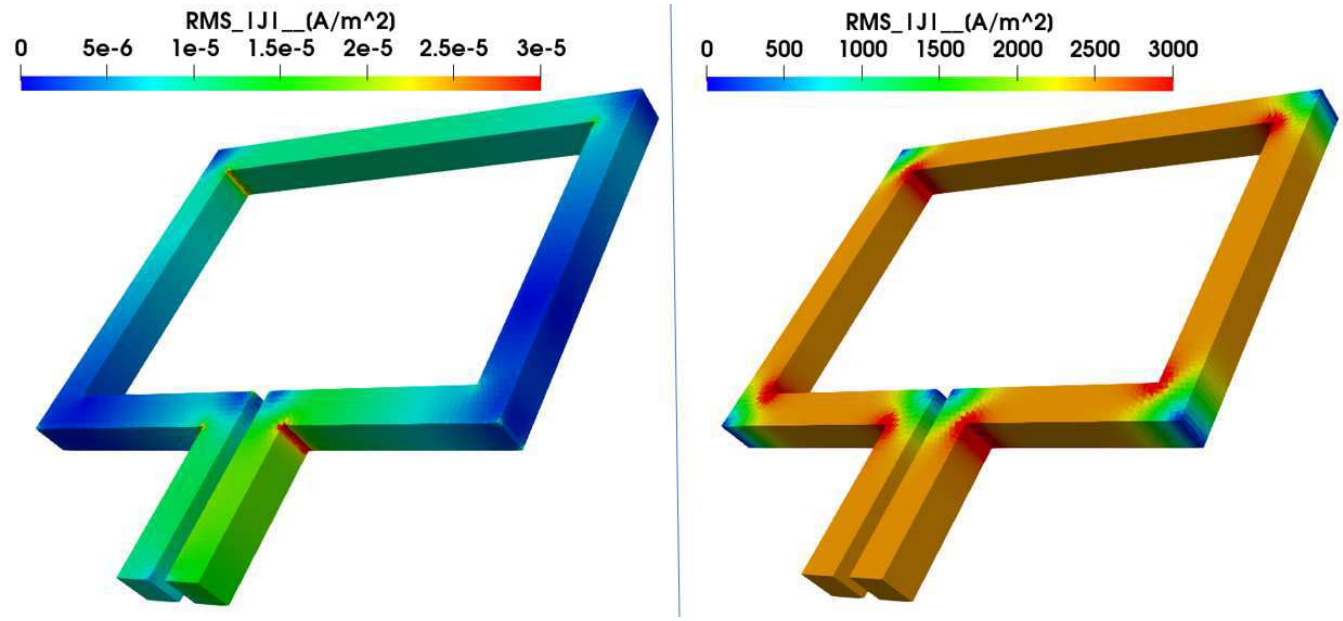

FIGURE 9 $f = 50\mathrm{Hz}$: RMS strength of electric currents in a cross-section of the conducting loop for two choices of topological cycle bounding in Ω: choice $\boldsymbol{\tau_2}$ **right**, choice τ_2' **left**, different scales used.

The simulation results compiled in Table 2 and displayed in Figure 9 strikingly highlight that the choice of topological cycles with respect to connector cycles is crucial. We offer the following interpretation of the data of Table 2: The choice τ_2 does not intersect the straight connector cycle between Γ_E^1 and Γ_E^2, directs the electromotive force $\dot{B}_1^T$ along the conducting part of the split loop and, hence, engenders a strong current. Conversely, choosing τ_2' forces the connector cycle γ_2^E to wind around the tunnel and confines the electromotive force to the air gap, where it cannot cause a significant current. The decreased current for larger frequencies is caused by the self-inductance of the conducting loop.

8 | CONCLUSION

We have discussed the most general case of the coupling of a linear full-Maxwell field model posed in a "field domain" with circuit models confined to a complementary "circuit domain" through non-local quantities associated with either ports (contacts, terminals) on the common interface of both domains or loops (tunnels, handles) of the circuit domain. We have rigorously derived how to obtain a computable discrete model through the following steps.

Identification of relative fundamental cycles on the interface	$\Rightarrow$	$\mathbf{E}$-based or $\mathbf{H}$-based variational formulations involving port/loop quantities	$\Rightarrow$	Finite-element Galerkin discretization

We have focused on variational formulations that directly involve the physical fields $\mathbf{E}$ and $\mathbf{H}$, thus circumventing the use of scalar and vector potentials. Our approach is suitable for both time and frequency domain.

This is the first work to highlight the complications inherent in a non-trivial topology of the circuity domain. If it features loops, numerical modeling entails making decisions about linked quantities. The single numerical example covered in this work gives a striking demonstration of unexpected interactions of loop and port quantities.

References

[1] Bossavit A. Most general "non-local" boundary conditions for the Maxwell equations in a bounded region. *COMPEL* 2000; 19(2): 239–245.

[2] Suuriniemi S, Kangas J, Kettunen L. Driving a coupled field-circuit problem. *COMPEL* 2007; 26(3): 899-909.

[3] Suuriniemi S, Kangas J, Kettunen L, Tarhasaari T. State variables for coupled circuit-field problems. *IEEE Transactions on Magnetics* 2004; 40(2): 949-952.

[4] Alonso Rodriguez A, Valli A. Voltage and current excitation for time-harmonic eddy current problems. *SIAM J. Appl. Math.* 2008; 68: 1477-1494.

[5] Hiptmair R, Sterz O. Current and voltage excitations for the eddy current model. *Int. J. Numer. Model* 2005; 18(1): 1-21.

[6] Ioan D, Schilders W, Ciuprina G, Meijs Nvd, Schoenmaker W. Models for integrated components coupled with their EM environment. *COMPEL: Int J for Computation and Maths. in Electrical and Electronic Eng.* 2008; 27(4): 820-829.

[7] Ciuprina G, Ioan D, Janssen R, van der Heijden E. MEEC Models for RFIC Design Based on Coupled Electric and Magnetic Circuits. *IEEE Transactions on Computer-Aided Design of Integrated Circuits and Systems* 2015; 34(3): 395-408.

[8] Ciuprina G, Ioan D, Popescu M, Lup S. Electric Circuit Element Boundary Conditions in the Finite Element Method for Full-Wave Frequency Domain Passive Devices. In: Mathematics in Industry. Springer; 2020. In print.

[9] Ciuprina G, Villena J, Ioan D, et al. Parameterized Model Order Reduction. In: Günther M., ed. *Coupled Multiscale Simulation and Optimization in Nanoelectronics*. 21 of *Mathematics in Industry*. Springer. 2015 (pp. 267-359)

[10] Dular P, Geuzaine C, Legros W. A Natural Method for Coupling Magnetodynamic H-Formulations and Circuit Equations. *IEEE Trans. Mag.* 1999; 35(3): 1626–1629.

[11] Dular P, Legros W, Nicolet A. Coupling of Local and Global Quantities in Various Finite Element Formulations and its Application to Electrostatics, Magnetostatics and Magnetodynamics. *IEEE Trans. Mag.* 1998; 34(5): 3078–3081.

[12] Dular P, Henrotte F, Legros W. A General and Natural Method to Define Circuit Releations Associated with Magnetic Vector potential Formulations. *IEEE Trans. Mag.* 1999; 35(3): 1630–1633.

[13] Bermúdez A, Rodríguez R, Salgado P. Numerical solution of eddy current problems in bounded domains using realistic boundary conditions. *Comput. Methods Appl. Mech. Engrg.* 2005; 194(2-5): 411–426.

[14] Bermúdez A, Piñeiro M, Rodríguez R, Salgado P. Analysis of an ungauged $T, \phi - \phi$ formulation of the eddy current problem with currents and voltage excitations. *ESAIM Math. Model. Numer. Anal.* 2017; 51(6): 2487–2509.

[15] Bermudez A, Lopez-Rdriguez B, Rodriguez R, Salgado P. An Eddy Current Problem In Terms Of A Time-Primitive Of The Electric Field With Non-Local Source Conditions. *Math. Model. Numer. Anal.* 2012. Submiited.

[16] Monk P. *Finite Element Methods for Maxwell's Equations*. Oxford, UK: Clarendon Press . 2003.

[17] Buffa A, Hiptmair R. Galerkin Boundary Element Methods for Electromagnetic Scattering. In: Ainsworth M, Davis P, Duncan D, Martin P, Rynne B., eds. *Topics in Computational Wave Propagation. Direct and inverse Problems*. 31 of *Lecture Notes in Computational Science and Engineering*. Berlin: Springer. 2003 (pp. 83-124).

[18] Hiptmair R, Kotiuga P, Tordeux S. Self-adjoint curl operators. *Annali di Matematica Pura ed Applicata* 2012; 191: 431-457.

[19] Flanders H. *Differential forms with applications to the physical sciences*. Academic Press, New York-London . 1963.

[20] Gross P, Kotiuga P. *Electromagnetic Theory and Computation: A Topological Approach*. 48 of *Mathematical Sciences Research Institute Publications*. Cambridge, UK: Cambridge University Press . 2004.

[21] Hiptmair R, Ostrowski J. Generators of $H_1(\Gamma_h, \mathbb{Z})$ for Triangulated Surfaces: Construction and Classification. *SIAM J. Computing* 2002; 31(5): 1405-1423.

[22] Kotiuga P. On making cuts for magnetic scalar potentials in multiply connected regions. *J. Appl. Phys.* 1987; 61(8): 3916–3918.

[23] Dł otko P, Specogna R, Trevisan F. Automatic generation of cuts on large-sized meshes for the T-Ω geometric eddy-current formulation. *Comput. Methods Appl. Mech. Engrg.* 2009; 198(47-48): 3765–3781.

[24] Kotiuga P. Topological duality in three-dimensional eddy-current problems and its role in computer-aided problem formulation. *J. Appl. Phys.* 1990; 9: 4717-4719.

[25] Hiptmair R. Finite elements in computational electromagnetism. *Acta Numerica* 2002; 11: 237-339.